https://doi.org/10.5194/egusphere-2025-2800
Preprint. Discussion started: 28 August 2025

Biogeochemical and absorption properties of different size fractions of suspended matter in the western Spitsbergen fjords (Svalbard Archipelago) in the summer

Justyna Meler[1], Joanna Stoń-Egiert[1], Monika Zabłocka[1]

[1]Institute of Oceanology Polish Academy of Sciences, Powstańców Warszawy 55, 81-712 Sopot, Poland

Correspondence to: Justyna Meler (jmeler@iopan.pl)

Abstract. In the summers of 2022 and 2023, the variability of biogeochemical properties and light absorption of suspended particulate matter (SPM) was investigated in three western Spitsbergen fjords: Hornsund, Kongsfjorden, and Isfjorden. Analyses included SPM and its organic (POM) and inorganic (PIM) fractions, chlorophyll *a* (Tchl*a*), and light absorption coefficients of total particles ($a_p(\lambda)$), phytoplankton ($a_{ph}(\lambda)$), and detritus ($a_d(\lambda)$). Measurements were conducted on unfractionated seawater and on size-fractionated samples obtained by cascade filtration, allowing the assessment of four particle classes: pico- (0.2–2 µm), ultra- (2–5 µm), nano- (5–20 µm), and micro-particles (20–200 µm).

The obtained results revealed clear differences in particle size contributions in the fjord waters. Ultra-particles dominated the total concentrations, contributing 39%–56% of SPM, POM, PIM, and Tchl*a*. Pico-particles also had large contribution: 16%–29%, and micro- and nano-particles accounted for 12%–17%. The average POM/SPM ratio was 33%, indicating the dominance of inorganic matter. However, organic contributions varied with size of particles: micro- and pico-particles contained more organic material (45% and 43%), while nano- and ultra-particles had lower proportions (38% and 26%).

Ultra-particles also played a leading role in light absorption at 443 nm, contributing 44%–62% to $a_p(443)$, $a_d(443)$, and $a_{ph}(443)$. Pico-, nano-, and micro-particles contributed 24%–28%, 10%–19%, and 4%–9%, respectively. Considerable variability in absorption properties was observed across size classes. Since variability ranges often overlap for different size classes, this may prevent unambiguous identification of particle size class based on light absorption spectra.

1 Introduction

Fjords are often called Aquatic Critical Zones due to their special significance in the context of climate change. They are regions where complex interactions occur between terrestrial, cryospheric, oceanic, and atmospheric processes within the Earth's climate system. As such, processes in fjord can provide information on the response of the system to changing environmental conditions (Bianchi et al., 2020). In recent decades, the Arctic Ocean and its catchment areas have undergone rapid changes associated with climate warming. Observations point to systematic increase in average air and water

https://doi.org/10.5194/egusphere-2025-2800
Preprint. Discussion started: 28 August 2025

temperatures in the fjords, making the Arctic one of the regions most affected by global warming (Pavlov et al., 2013). Warming in the Arctic leads to a rapid reduction in sea ice, melting of glaciers and increased river runoff causing physical and biogeochemical changes in its water masses (Meier et al., 2014), including those in the fjords of West Spitsbergen (Błaszczyk et al., 2013). Changes in ocean acidification, nutrient concentration levels, and shift in phytoplankton community structure have also been observed (Gao et al., 2019; Rousseaux and Gregg, 2015; Tate et al., 2017).

The West Spitsbergen fjords are located in a key water mass interaction area (Figure 1), where Atlantic water (AW) transporting heat and salt to the Arctic Ocean meets colder polar waters (Schauer et al., 2004; Walczowski and Piechura, 2007). More than 30% of the total AW reaches the Arctic through the Fram Strait via the West Spitsbergen Current (WSC) (Beszczyńska-Möller et al., 2012), which is a northern branch of the Norwegian Atlantic Current (NAC). At approximately 79°N, the WSC splits into two branches: the Svalbard Branch (SB) and the Yermak Plateau Branch (YPB). The West Spitsbergen fjords are partially separated from the WSC by the Sørcapp Current (SC), an extension of the East Spitsbergen Current (ESC) which transports cold Arctic Water (ArW) from the Barents Sea along the West Spitsbergen Shelf (WSS) northward. Mixing of WSC and SC waters along the polar front, combined with atmospheric processes (heating and cooling), freeze-thaw cycles, precipitation and evaporation (Walczowski, 2013; Saloranta and Svendsen, 2001), cools the WSC on its way north. As a result, the water mass flowing into the fjords is colder and less saline.

Three major fjords: Kongsfjorden, Isfjorden and Hornsund – are located along the west cost of Spitsbergen. Due to lack of distinct sills, AW water can freely enter them. The depth of the entrance section of Kongsfjorden reaches almost 400 m, Isfjorden up to 450 m, while Hornsund is rather flat and relatively shallow, approximately 150 m. The variability of temperature and salinity in the three considered fjords depends on the mutual influence and strength of the Sørkapp Current (SC) and the West Spitsbergen Current (WSC). Consequently, Hornsund, located closer to the Sørkapp Current, is generally colder and has features of Arctic-type fjords compared to Isfjorden and Kongsfjorden (Promińska et al., 2017).

The biogeochemical and optical properties of fjord waters are strongly related to biological productivity and the inflow of suspended matter of terrestrial and glacial origin (D'Sa, Miller and Del Castillo, 2006; Lund-Hansen et al., 2010; Szeligowska et al., 2021; Assmy et al., 2023; Chitkara et al., 2024). The main factors influencing the variability of optical properties of fjord waters are glacier melting, river discharge , and the seasonal cycle of biological activity (Smoła et al. 2017; Sagan and Darecki, 2018; Halbach et al. 2019; Pavlov et al. 2019; Skogseth et al. 2020). In winter, due to the lack of light, biological activity is significantly reduced (Granskog et al. 2014, 2015). In spring and summer, meltwater from tidal glaciers becomes the main source of freshwater in fjords (Błaszczyk et al., 2019), accompanied by snowmelt, precipitation, groundwater drainage, and runoff from rivers that are fed by melting snow and glacier ice (Cottier et al., 2005). The seasonal influx of meltwater typically begins in June, peaks in July–August, and ends around September (Darlington, 2015). Melting glacier water carries large amounts of sediment particles, which create strong salinity and turbidity gradients (Pavlov et al., 2019). The freshwater influx often increase nutrients levels, which leads to an increase in phytoplankton - mainly in spring and late summer (Assmy et al., 2023; Chitkara et al., 2024).

https://doi.org/10.5194/egusphere-2025-2800
Preprint. Discussion started: 28 August 2025

In fjord waters composition of suspended particulate matter (SPM) addicted to physical factors (e.g., tides, glacial melt, inflow of river waters) and biogeochemical processes (e.g., phytoplankton blooms) (D'Sa and Ko, 2008; Eleveld et al., 2014). Fjords exhibit high levels of mineral particles due to meltwater and river inflows, (Dragańska-Deja, 2024), along with lithogenic particles responsible for changes in benthic communities (Braeckman et al., 2021; Clark et al., 2017; Deja et al., 2016) and plankton distribution (Deja et al., 2019; Szeligowska et al., 2021, 2022). Phytoplankton biomass near glacier fronts has been linked to the underlying bedrock composition (Halbach et al., 2019).

The diversity of particle types and sources in the marine environment leads to variations in absorption properties across time and space. Particulate organic matter (POM) includes both living and non-living components, such as microalgae, bacteria, and mineral clays (Volkman & Tanoue, 2002). Living POM is essential for marine food webs and ocean biogeochemical cycles, participating in key processes like photosynthesis, nitrogen fixation, and remineralization (Voss et al., 2013). In contrast, non-living POM is chemically dominated by complex and refractory carbohydrates, which contribute to a larger pool of accumulated biomass compared to living POM. The size of suspended particles strongly influences their residence time in the water column. Large particles sink more rapidly in water, and undergo different transformations before reaching the seabed. Sedimentation process represents the primary pathway of carbon transport below the euphotic zone through the biological carbon pump (Turner et al., 2015). However, precise characterization of inherent optical properties (IOPs) remains difficult in optically complex waters where the proportions of organic and inorganic matter vary (McKee & Cunningham, 2006; Davies et al., 2014).

Knowledge of the size structure of phytoplankton populations and the role of mineral and detritus particle sizes on light absorption is essential to better determine the impact of climate change on coastal marine systems (e.g. Le Quéré et al., 2005; Stramski et al., 2007; Woźniak and Stramski, 2004). Suspended particles –phytoplankton, detritus and mineral particles – are different in their light absorption spectra. The light absorption coefficient of suspended phytoplankton organisms, $a_{ph}(\lambda)$, is related to the pigment composition of the algal cells, and its spectral shape has two characteristic maxima (around 400–490 nm and 660–690 nm). The light absorption coefficient spectrum of detritus and mineral particles, $a_d(\lambda)$, is characterized by a monotonic exponential-shaped decline (Morel and Bricaud, 1981; Sathyendranath et al., 1987; Ciotti et al., 2002; Woźniak and Dera, 2007).

The size and taxonomy of phytoplankton can be inferred from the spectral coefficient $a_{ph}(\lambda)$ values. Direct measurements of the light absorption coefficients of suspended particles provide fundamental basis for estimating the size structure of phytoplankton populations (Organelli et al., 2013; Zhang et al., 2015). According to Ciotti et al. (2002) more than 80% of the variability in $a_{ph}(\lambda)$ can be explained as a combination of the dominant size class and the variability of pigments present in the studied particles. However, the waters of Spitsbergen fjords are typically dominated by detritus particles and mineral particles (Szeligowska et al., 2021; Dragańska-Deja, 2024; Woźniak et al., 2024a and b). The assessment of the influence of the size of suspended particles on their absorption properties can be performed by physically separating fractions of different sizes of suspended particles and measuring the light absorption coefficients for these separated fractions (Ciotti et al., 2002; Meler et al., 2023; Woźniak et al., 2024b).

https://doi.org/10.5194/egusphere-2025-2800
Preprint. Discussion started: 28 August 2025

The aim of our study was to determine the variability of biogeochemical properties of suspended particles (SPM, POM, PIM, POM/SPM, Tchl*a*) and spectral absorption coefficients of light, by different size fractions (obtained by cascade filtration of large volumes of water samples through a system of nylon meshes and filters with specific pore sizes) of suspended particles (a_p) (divided into phytoplankton, a_{ph}, and detritus and mineral particles, a_d) present in the waters of three selected fjords of Spitsbergen. The studies were carried out for original water samples and for four particle size fractions, conventionally defined as follows: micro-particles (approximately 20–200 µm), nano-particles (5–20 µm), ultra-particles (2–5 µm), and pico-particles (0.2–2 µm). This classification follows the scheme proposed by Sieburth et al. (1978) and Ciotti et al. (2002). Micro-particles, which are mainly represented by diatoms and dinoflagellates, play a key role at higher trophic levels (zooplankton and fish) and contribute to blooms that cause short-term increases in primary production. The size and cellular structure of micro-particles facilitates the rapid sinking of organic carbon, contributing to biological carbon pump (Guidi et al.2009; IOCCG, 2014). Nano- and ultra-particles, mainly represented by small flagellates and coccolithophores, are an important link between the classical food web and the microbial loop (Ward et al., 2012; IOCCG, 2014). Nano- and ultraphytoplankton efficiently utilize dissolved nutrients in water and play an important role in the carbon cycle by producing calcium-carbonate shells that increase carbon export during sedimentation (Balch et al., 2011; IOCCG, 2014). Pico-particles, mainly cyanobacteria and small eukaryotic phytoplankton, contribute significantly to primary production (Ciotti et al. 2002; IOCCG, 2014).

The detailed objectives of our analyses are: 1) to determine the contribution of particle size classes to the total concentrations of suspended matter (SPM) and its organic (POM) and inorganic (PIM) fractions as well as the total concentration of chlorophyll *a* (Tchl*a*), 2) to determine the contribution of particle size classes in the total light absorption by all particles, phytoplankton and detritus + mineral particles, 3) to determine the average specific light absorption coefficients (i.e. light absorption coefficients normalized to the SPM or Tchl*a* concentration) for particular size classes.

Each particle size class plays a distinct role in the marine environment, therefore studying the distribution and variability of different particle size fractions is crucial for understanding the complex interactions in marine ecosystems. From these studies, it is possible to estimate the size structure of phytoplankton populations, their response to environmental changes, and the contribution of individual particle size fractions to global carbon and nutrient cycles. The analytical results presented in this paper are necessary to create algorithms whose task is to recover physical, biological and chemical data from satellite maps, especially regional algorithms for marine ecosystems characterized by complex optical properties, such as Arctic fjords.

2 Materials and methods

2.1 Description of study area and water samples

The study was conducted in three fjords of West Spitsbergen (Hornsund, Kongsfjorden and Isfjorden) during the summer season (late July–August) of 2022 and 2023, on board r/v Oceania (Figure 1a). These fjords are strongly influenced by two major ocean currents: the Sørkapp Current (SC), carrying cold Arctic Water (ArW) from the Barents Sea, and the West Spitsbergen Current (WCS), carrying warmer and saltier AW from the Norwegian Sea (Promińska et al., 2018). The inflow of

https://doi.org/10.5194/egusphere-2025-2800
Preprint. Discussion started: 28 August 2025

AW accelerates ice melting and has a significant impact on biogeochemical cycles and nutrient dynamics (Hegseth et al., 2019; Konik et al., 2021). The water masses in Hornsund are strongly shaped by SC, while in Isfjorden and Kongsfjorden the influence of AW transported by WSC plays a more important role. Within the fjords, surface water (SW) is formed locally by glacial melt and river runoff (Skogseth et al., 2020). The Svalbard fjords are typically characterized by a three-layer structure: surface water (formed location), intermediate water (advective water occurring at intermediate depths) and winter water (occupying the deepest layers if the water column) (Cottier et al., 2010). The surface layer, with its relatively low salinity, originates mainly from sea ice and glacier melt, as well as freshwater runoff discharged in spring and early summer. The gradual formation of a density gradient limits vertical mixing and sedimentation of particles. Suspended and dissolved material trapped in the surface layer accelerate water heating during the months with the strongest sunlight (June to August), creating optimal conditions for phytoplankton development and primary productivity (Calleja et al. 2017; Konik et al., 2021).

Hornsund, located at the southern tip of Spitsbergen, is approximately 30 km long and 15 km wide (Fig.1a and b). It is characterized by high nutrient enrichment and is strongly influenced by cold Arctic waters (ArW) and cold coastal waters (Włodarska-Kowalczuk et al., 1998; Saghravani et al., 2024). These factors make the primary productivity in Hornsund higher compared to other fjords (Santos-Gracia et al., 2022). The surface waters of the fjord are strongly influenced by melting glacier and river waters (Zaborska et al. 2020).

Kongsfjorden, located at 79°N on the west coast of the Svalbard archipelago, is about 20 km long and up to 10 km wide (Fig.1a and b). Unlike other Arctic fjords, Kongsfjorden is subject to intensive advective inflow of warm and salty AW waters into the fjord throughout the year (Cottier et al., 2007; Pavlov et al., 2019). Fjord water dynamics result from opposing processes – inflow of AW and ArW on one hand, and water from the melting glacier on the other (Halbach et al., 2019; Saghravani et al., 2024). The effect of this interaction is the intensification of nutrient and carbon cycling, increased primary productivity and periodic oxygen depletion in deeper water layers (Santos-Garcia et al., 2022).

Isfjorden is the largest fjord system on Spitbergen - about 100 km long and on average about 24 km wide (Fig.1a and b). It is under the continuous influence of AW (Pavlov et al., 2014; Skogseth et al., 2020). The seasonal stratification occurring in the fjord is responsible for the retention of nutrients in the euphotic zone and limitation of vertical mixing in the most productive season (McGovern et al., 2020; Finne et al., 2022). In addition, increased river freshwater inflow, especially in summer, provides additional nutrients influencing biogeochemical processes (Saghravani et al., 2024).

https://doi.org/10.5194/egusphere-2025-2800
Preprint. Discussion started: 28 August 2025

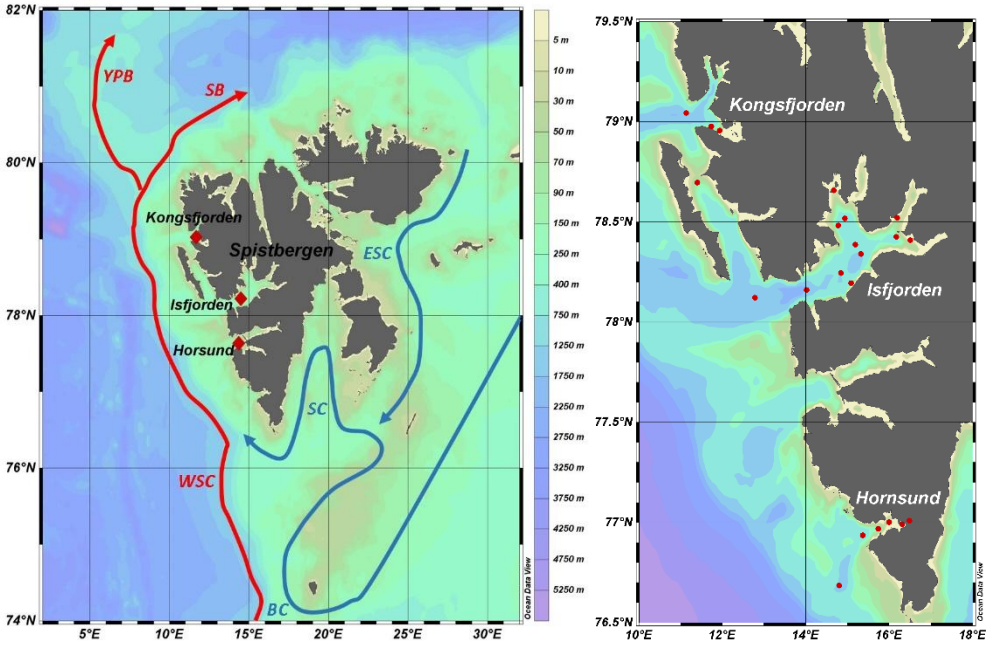

Figure 1: Study area including map of Spitsbergen with main currents (a): West Spitsbergen Current (WSC), and East Spitsbergen Current (ESC) drawn with red and blue arrows, respectively. WSC separate into two branches: Svalbard Branch (SB) and Yermak Branch (YB). ESC continues as Spitsbergen Current (SC) west of Svalbard (according to Skogseth et al. (2020)), BC - Bjørnøja Current. Red dots indicates location of measurement stations in the fjords of Spitsbergen (b).

The locations of the measurement stations (Fitg.1b) in our study were selected to capture the greatest possible optical diversity of fjord waters. The studies were conducted in three fjords of Spitsbergen. In Hornsund, measurements were carried out from July 31 to August 3, 2022 (at 6 stations), and from July 27 to July 31, 2023 (at 3 stations). In Kongsfjorden, measurements were performed in the periods from 7 to 11 August 2022 (at 3 stations) and from 5 to 8 August 2023 (at 4 stations). In Isfjorden, measurements were performed from 15 to 25 August 2022 (at 9 stations) and from 12 to 18 August 2023 (at 6 stations). At each station, basic water characteristics were measured (water transparency using a Secchi disk, temperature, and salinity). Sea water transparency measured with the Secchi disk in Hornsund ranged from 1 m to 10 m, in Kongsfjorden from 1.5 m to 7.5 m, and in Isfjorden from 2 m to 12 m. Water temperature and salinity varied in individual regions as follows: 2.9 – 6.6 ^{0}C and 30.3 – 34.1 in Horsund, 3.8 – 8.5 ^{0}C and 28.0 – 34.1 in Kongsfjorden, and 6.0 – 9.6 ^{0}C and 27.5 – 33.1 in Isfjorden. This values indicate that the measured water masses predominantly belonged to the surface water layer (T>0, Sal<34 (Promińska et al. 2018)).

https://doi.org/10.5194/egusphere-2025-2800
Preprint. Discussion started: 28 August 2025

2.2 Processing of water samples

The dataset consists of 31 data sets collected during 2 research cruises on board R/V Oceania in 2022 and 2023 conducted in the western Spitsbergen region. Seawater samples were processed using cascade filtration to separate suspended particles into size fractions. Filtration was performed through filters/filter meshes with different pore sizes (20 µm, 5 µm, 2 µm). A detailed description of the cascade filtration is presented in Meler et al. (2023).

Original seawater samples were collected and sequentially filtered to obtain three filtrates: filtrate A (water filtered through 20 µm nylon mesh), filtrate B (filtrate A further filtered through 5 µm nylon meshes) and filtrate C (filtrate B furthered filtered through 2 µm membrane filters). Subsequently, additional filtration was performed to determine a number of physicochemical parameters in the original sample and in each of the filtrates. These were: SPM concentrations (g m^{-3}) (including organic matter (POM) and inorganic matter (PIM)), Tchl*a* concentrations (mg m^{-3}) and samples needed to determine the values of light absorption coefficients by all suspended particles ($a_p(\lambda)$, m^{-1}), detritus ($a_d(\lambda)$, m^{-1}) and phytoplankton ($a_{ph}(\lambda)$, m^{-1}) in all distinguished size classes (micro-particles, nano-particles, ultra-particles and pico-particles).

The values of particular biogeochemical and optical parameters in all distinguished size classes were determined following the methodology described in Meler et al. (2023) and Ciotti et al., (2002). The micro-particles were defined as the difference between the original water sample and fraction A. The nano-particles were defined as the difference between fraction A and fraction B; ultra-particles were defined as the difference between fraction B and fraction C, while pico-particles were represented by fraction C.

2.3 Parameters describing suspended particulate matter

The concentrations of suspended particulate matter (SPM, g m^{-3}), along with its organic (POM) and inorganic (PIM) fractions, were measured using the gravimetric method and the loss-on-ignition technique, following the procedures outlined by Woźniak et al. (2018) and Pearlman et al. (1995). A detailed description of the methods is presented in Meler et al. (2023). The SPM concentration values for seawater filtrates (original and fractions A, B and C) were calculated based on the difference in mass between filters containing collected suspensions and clean filters. POM values were obtained from subtracting the weights of filters with suspension after combustion from the weight before combustion. PIM was calculated as the difference between SPM and POM. Both, SPM and POM values were also corrected using reference filters.

The concentrations of particular phytoplankton pigments were determined using the reverse-phase high-performance liquid chromatography (HPLC-RP) method according to the methodology described in detail in the works of Stoń-Egiert and Kosakowska (2005) and Meler et al. (2017). The concentrations of 21 pigments identified in the samples, the total concentrations of chlorophyll *a* (Tchl*a*, mg m^{-3}) (defined as the sum of the concentrations of chlorophyll *a*, optical isomers of chlorophyll *a* and unidentified derivatives of chlorophyll *a*), the total content of chlorophyll *b* and its derivatives (Tchl*b*, mg m^{-3}), chlorophyll *c* and its derivatives (Tchl*c*, mg m^{-3}), the total content of photosynthetic carotenoids (PSC, mg m^{-3}) and photoprotective carotenoids (PPC, mg m^{-3}) were determined.

https://doi.org/10.5194/egusphere-2025-2800
Preprint. Discussion started: 28 August 2025

2.4 Light absorption by suspended particles and dissolved organic matter

The light absorption coefficient spectra of particles suspended in seawater, $a_p(\lambda)$ (m^{-1}), and of detritus, $a_d(\lambda)$ (m^{-1}), for the original samples and fractions A, B and C were measured using a Perkin-Elmer Lambda 650 spectrophotometer equipped with an integrating sphere of 150 mm diameter. Seawater samples for these analyses were obtained by filtering small volumes of seawater (from 80 mL for the original water samples to 2300 mL for fraction C) through Whatman filters (GF/F, 25 mm). Spectrophotometric measurements were performed inside the integrating sphere (Stramski et al., 2015; Woźniak et al., 2022; Meler et al., 2023), in the spectral range of 290-860 nm for filters with suspended matter and for the same filters bleached with 2% sodium hypochlorite $NaClO_2$ solution (Meler et al., 2020). The coefficients $a_p(\lambda)$ and $a_d(\lambda)$ were determined, and from their difference the phytoplankton light absorption coefficients ($a_{ph}(\lambda)$, (m^{-1})) were determined.

The light absorption coefficient spectra of chromophoric dissolved organic matter, $a_{CDOM}(\lambda)$ (m^{-1}), were determined spectrophotometrically using a Perkin-Elmer Lambda 650 spectrophotometer according to the methodology described by Meler et al. (2023).

3 Results and discussion

3.1 Variability in the biogeochemical characteristics of suspended matter

The dataset shows high variability of biogeochemical parameters in both original water samples and specific size classes. The classification was based on the phytoplankton size categories according to Ciotti et al. (2002), which define four classes: micro-particles (20-200 µm), nano-particles (5-20 µm), ultra-particles (2-5 µm) and pico-particles (<2 µm). Table 1 presents the mean values of SPM, POM, PIM and Tchl*a*, as well as the ratios of POM/SPM and Tchl*a*/SPM, together with the standard deviations (SD) and the minimum and maximum values. For the entire dataset, the variability of SPM concentrations ranged from 0.56 to 12.14 g m^{-3} and Tchl*a* concentrations from 0.27 to 2.13 mg m^{-3} for the original water samples.

Table 2: Variability of parameters describing suspended matter in seawater (mean ± standard deviation (SD), and range of variation) in all data and in particular fiords

quantity	SPM [g m^{-3}]	POM [g m^{-3}]	PIM [g m^{-3}]	Tchl*a* [mg m^{-3}]	POM/SPM	Tchl*a* /SPM
original samples (all particles)						
average ± SD	2.47 ± 2.09	0.63± 0.33	1.84 ± 1.81	0.91 ± 0.62	0.33 ± 0.15	0.0007 ± 0.0006
min – max (n=31)	0.56-12.14	0.23-2.13	0.12-10.01	0.27-3.20	0.13-0.78	0.0001-0.0022
micro-particles (20-200 µm)						
average ± SD	0.31 ± 0.41	0.12 ± 0.15	0.19 ± 0.28	0.12 ± 0.13	0.45 ± 0.35	0.001 ± 0.0023

https://doi.org/10.5194/egusphere-2025-2800
Preprint. Discussion started: 28 August 2025

min – max (n=31)	0-2.15	0-0.74	0-1.41	0-0.42	0-1.32	0-0.0082
			nano-particles (5-20 µm)			
average ± SD	0.42 ± 0.70	0.12 ± 0.14	0.31 ± 0.58	0.14 ± 0.17	0.38 ± 0.26	0.0008 ± 0.0013
min – max (n=31)	0-3.93	0-0.61	0-3.318	0-0.75	0-1	0-0.0051
			ultra-particles (2-5 µm)			
average ± SD	1.36 ± 1.44	0.25 ± 0.22	1.11 ± 1.24	0.43 ± 0.45	0.26 ± 0.16	0.0008 ± 0.001
min – max (n=31)	0.24-7.61	0-1.33	0.05-6.28	0-2.34	0-0.81	0-0.0047
			pico-particles (<2 µm)			
average ± SD	0.37 ± 0.18	0.14 ± 0.06	0.24 ± 0.17	0.26 ± 0.20	0.43 ± 0.22	0.0009 ± 0.0008
min – max (n=31)	0.08-0.91	0.05-0.24	0-0.73	0.04-0.86	0.14-0.99	0.0001-0.0034
			Hornsund (all particles)			
average ± SD	3.79 ± 3.14	0.74 ± 0.50	3.05 ± 2.68	0.67 ± 0.39	0.24 ± 0.12	0.0003 ± 0.0002
min – max (n=9)	1.18-12.14	0.36-2.13	0.59-10.01	0.27-1.54	0.13-0.50	0.00007-0.0008
			Konsfjorden (all particles)			
average ± SD	1.84 ± 0.90	0.53 ± 0.10	1.31 ± 0.86	1.29 ± 0.93	0.37 ± 0.20	0.0012 ± 0.0001
min – max (n=7)	0.56-3.43	0.40-0.69	0.12-2.78	0.27-3.20	0.17-0.78	0.0001-0.0022
			Isfjorden (all particles)			
average ± SD	1.97 ± 1.109	0.60 ± 0.24	1.37 ± 0.95	0.88 ± 0.44	0.36 ± 0.12	0.0006 ± 0.0005
min – max (n=15	0.61-4.02	0.23-1.21	0.31-3.46	0.46-2.15	0.14-0.54	0.0002-0.0019

Figure 2 shows the average relative contributions of SPM, POM, PIM and Tchl*a* in a given size class to the total SPM, POM, PIM or total Tchl*a* for individual samples in the different sampling areas: Hornsund, Kongsfjorden and Isfjorden.

The first part of Table 2 shows the contributions of SPM in size classes to the total SPM for all data and divided into sampling regions. In the analyzed data set, ultra-particles had a dominant contribution in the total SPM, on average 50%. Pico-particles had a contribution of about 19%, micro-particles – 16%, and nano-particles – 14% (Figure 2a). The variability of particles defined as micro-particles for all data was 0-75%. The contribution of nano-particles ranged from 0 to 46%, of ultra-particles

https://doi.org/10.5194/egusphere-2025-2800
Preprint. Discussion started: 28 August 2025

from 12 to 78.5%, and of pico-particles from 2.6 to 45%. The average contribution of micro-particles in Hornsund and Kongsfjorden was about 13%, in Isfjorden it was slightly higher – 19%. The highest average contribution of nano-particles was observed in Hornsund (18%), and in the other fjords about 12.5%. The contribution of ultra-particles in Hornsund and Kongsfjorden was 53%, and in Isfjorden 48%, while the contribution of pico-particles in Kongsfjorden and Isfjorden was 21% and in Hornsund 15.5%.

Figure 2b and 2c show the contribution of POM and PIM in the individual size classes. The average contribution of POM in a given size class to total POM for all data is highest for ultra-particles (39.5%, 0–66%), followed by pico-particles (25%, 5–64%), while the average contribution of POM in the micro- and nano-particle classes was 19% (0–61%) and 16.5% (0–51%), respectively. In different fjords the variability of POM contribution in particular size classes was recorded. In the samples from Hornsund, the highest proportions of POM were found in the ultra (43%) and nano (20.6%) size classes and the lowest proportions of micro- and pico-particles (20.5%). In Kongsfjorden, the highest proportion of POM was found in ultra-particles (40%), followed by pico-particles (26.5%), while micro- and nano-particles had lower proportions of POM (16% and 17%, respectively). The waters of Isfjorden were characterized by the highest proportions of POM in the ultra (37%) and pico (27%) size classes, lower proportions of POM in the micro (22%) and nano (14%) size classes. The suspended matter were dominated by inorganic matter (Figure 2c).

Figure 2d shows the contribution of Tchl*a* in the individual size fractions. The average Tchl*a* proportion in a given size class relative to the total Tchl*a* for all data was highest for ultra-particles (47%) and pico-particles (29%), while the average Tchl*a* contribution in the nano- and micro-particle classes was about 12% (Table 2). Variability in the Tchl*a* contribution in the size classes was observed in the particular fjords. The highest Tchl*a* contribution was found everywhere in ultra-particles, in Hornsund (55%, 0-82%), in Isfjorden (47%, 19.5-75%) and in Kongsfjorden (36%, 0-73%). High average Tchl*a* proportions were recorded in Kongsfjorden in the pico-particle class (41%, 25-68%) and in Isfjorden (30.6%, 11-47%), while in Hornsund it was lower (18%, 8-29%). The average Tchl*a* contribution in the micro- and nano-particle classes were similar in the analysed fjords and varied from 10 to 14%.

https://doi.org/10.5194/egusphere-2025-2800
Preprint. Discussion started: 28 August 2025

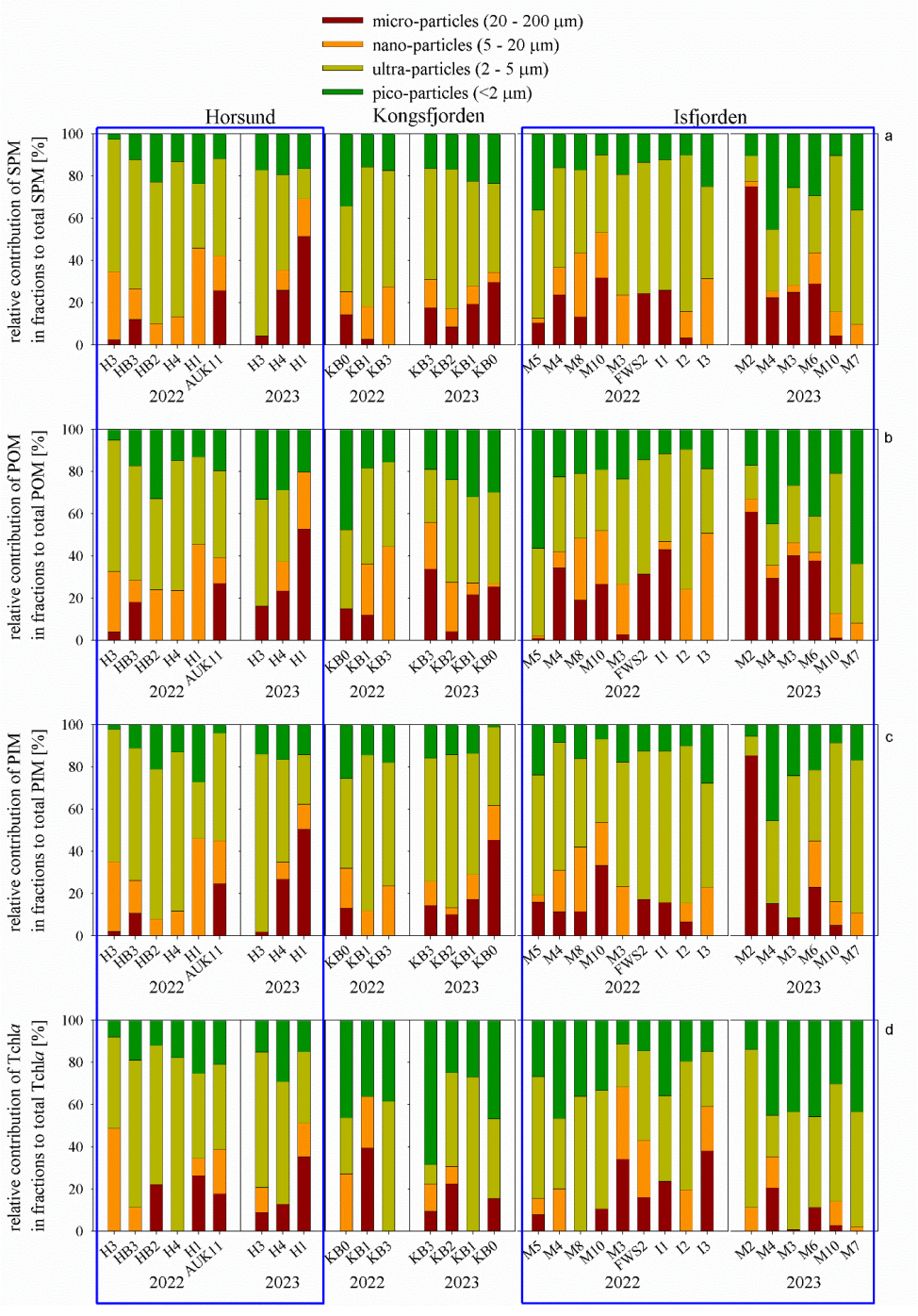

Figure 2: Relative contributions of suspended particulate matter (SPM) in selected fractions to total SPM (a), particulate organic matter (POM) to total POM (b), particulate inorganic matter (PIM) to total PIM (c), and total chlorophyll *a* (Tchl*a*) to total Tchl*a* (d), presented by region (Hornsund, Kongsfjorden, Isfjorden).

https://doi.org/10.5194/egusphere-2025-2800
Preprint. Discussion started: 28 August 2025

Table 2: Contributions of different particle size classes (micro, nano, ultra, pico) to total SPM, POM, PIM, and TChl*a* (n=31). Data are presented as mean ± SD with ranges, for the entire dataset and by sampling area.

	all data	Hornsund	Kongsfjorden	Isfjorden
SPM_{micro}/SPM	16.2 % ± 16.7 % 0-75.1%	13.6 % ± 16.7 % 0-51.4%	13.2 % ± 9.6 % 0-29.8 %	19.3% ± 18.6 % 0-75.1 %
SPM_{nano}/ SPM	13.9% ± 10.8 % 0-46 %	17.8 %± 12.8 % 0- 46 %	12.9 % ± 6.9 % 4.8 % - 27.7 %	12 % ± 10.2 % 0- 31.3 %
SPM_{ultra}/ SPM	50.5 % ± 16.6 % 12 % -78.5 %	53.2 % ± 19.9 % 14.1 %-78.5 %	53.1 % ± 9.5 % 40.5 % - 66 %	47.7 % ± 16.7 % 12 % - 74 %
SPM_{pico}/ SPM	19.4 % ± 9.2 % 2.6 %-45.2 %	15.5 % ± 6.1 % 2.6 % - 23.6 %	20.9 % ± 6.2 % 15.6 % - 34.3 %	21 % ± 11 % 9.8 % - 45.2 %
POM_{micro}/ POM	18.8 % ± 17.2 % 0-60.9 %	15.7 % ± 16.5 % 0-52.8 %	16 % ± 11 % 0-33.8 %	21.9 % ± 19.2 % 0-60.9 %
POM_{nano}/ POM	16.6% ± 13.8 % 0-50.7 %	20.6 % ± 12.3 % 0- 45.5 %	17.3 % ± 14.8 % 0- 44.5%	13.9 % ± 13.5 % 0-50.7 %
POM_{ultra}/ POM	39.5 % ± 15.1 % 0-66.4 %	43.2 % ± 17.8 % 0 – 62.4 %	40.1 % ± 6.2 % 25.3 % - 48.5 %	36.9 % ± 15.7 % 16 % - 66.4 %
POM_{pico}/ POM	25.2 % ± 13.3 % 5 % - 63.7 %	20.5 % ± 9 % 5 % - 33.1 %	26.5 % ± 10.2 % 15.5 % - 47.5 %	27.3 % ± 15.9 % 9.5 % - 63.7 %
PIM_{micro}/ PIM	15 % ± 18.2 % 0-85.4 %	12.9 % ± 16.6 % 0-50.4 %	14.3 % ± 14.2 % 0-45.5 %	16.6 % ± 20.4 % 0-85.4 %
PIM_{nano}/ PIM	13.7% ± 11.9 % 0 – 46.1 %	17.2 % ± 13.4 % 0- 46.1 %	13.9 % ± 6 % 3.4 % - 23.8%	11.5 % ± 10.4 % 0-30.5 %

https://doi.org/10.5194/egusphere-2025-2800
Preprint. Discussion started: 28 August 2025

PIM_{ultra}/ PIM	55.7% ± 17.7 % 9.1 % - 84.2 %	56.2 % ± 19.6 % 23.6 % - 842 %	57.2 % ± 12.7 % 37.3 % - 73.8 %	54.7 % ± 12.7 % 9.1 % - 75.1%
PIM_{pico}/ PIM	15.5 % ± 8.8 % 1.1 % - 45.5 %	13.6 % ± 7.3 % 2.1 % - 27 %	14.6 % ± 6.7 % 1.1 % - 25.5 %	17.1 % ± 10.1 % 5.5 % - 45.5 %
Tchla_{micro}/ Tchl*a*	12.1 % ± 12.7 % 0-39.3 %	13.7 %± 12 % 0-35.4 %	12.4%± 13.7 % 0-39.3 %	11.1 %± 12.5 % 0-38.1 %
Tchla_{nano}/ Tchl*a*	11.6% ± 12 % 0-48.8 %	13 %± 14.5 % 0- 48.8 %	10.4 %± 10.8 % 0- 27.2%	11.3 %± 10.8 % 0-34.2 %
Tchla_{ultra}/ Tchl*a*	47 % ± 19.4 % 0-82.2 %	55.4 %± 15. % 34 % - 82.2 %	36.1 %± 24.5 % 0- 73.1 %	47 %± 16 % 19.5 % - 74.9 %
Tchla_{pico}/ Tchl*a*	29.3 % ± 14.1 % 7.9 % - 68.4 %	17.9 %± 6.2 % 7.9 % - 29 %	41.1 %± 13.6 % 24.8 % - 68.4 %	30.6 %± 12.6 % 11.1 % - 46.6 %

In the original samples, the POM/SPM ratio (reflecting the proportion of organic matter in total suspended matter) varied between 0.13 and 0.78 (Figure 3). The highest POM/SPM variability was observed in Kongsfjorden (0.17-0.78). In Hornsund and Isfjorden, the POM/SPM variability was lower (0.13-0.54). Analyses of the POM/SPM ratio in particular size classes show similar variability, where with the increase in the SPM, the proportion of organic particles in the suspended matter decreases. For the all data set, the highest POM/SPM proportion was observed for micro-particles and pico-particles, on average about 45%, then for nano-particles - 38% and the lowest for ultra-particles - 26%.

https://doi.org/10.5194/egusphere-2025-2800
Preprint. Discussion started: 28 August 2025

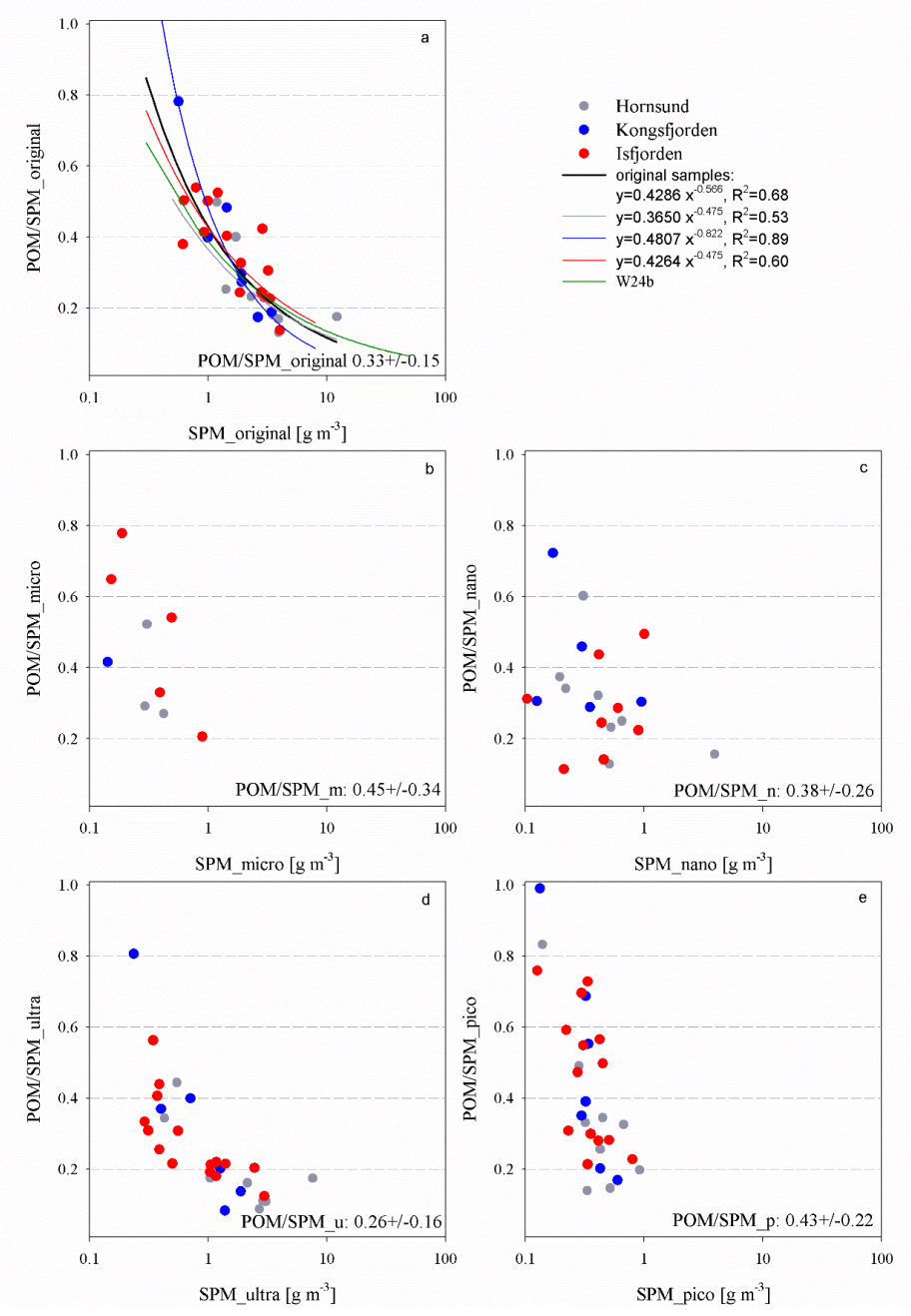

Figure 3: Relationships between the POM/SPM ratio and the SPM concentration for the original water samples (a) and in the size classes: micro (b), nano (c), ultra (d) and pico (e) (grey dots – Hornsund, blue dots – Kongsfjorden, red dot – Isfjorden). Mean values ± standard deviation are shown in the graph. The relationships are shown for the all dataset (black line), W24b - Woźniak et al. (2024b) (green line), and separately for the fjords: Hornsund (gray line), Konsfjorden (blue line) and Isfjorden (red line).

https://doi.org/10.5194/egusphere-2025-2800
Preprint. Discussion started: 28 August 2025

3.2 Variability of diagnostic pigments

HPLC analysis of the water samples in the analyzed data set allowed the identification of 21 phytoplankton pigments. Figure 4 shows the ranges of variability of selected pigments considered as taxonomic markers of phytoplankton (Sieberth et al., 1978; Vidussi et al., 2001). Peridinin (peri) is considered a marker of dinoflagellates, and fucoxanthin (fuko) a marker of diatoms (both phytoplankton populations considered as microphytoplankton (Uitz et al., 2006; Hirata et al., 2008)). 19'hex-fucoxanthin (19'hex) indicates the presence of prymnesiophytes, 19'but-fucoxanthin (19'but) – chrysophytes, alloxanthin (allo) is a marker of cryptophytes, and chlorophyll *b* (Tchl*b*) – green algae (three phytoplankton populations considered nanoplankton; Hirata et al. 2008). Zeaxanthin (zea) is a marker of cyanobacteria classified as picophytoplankton (Uitz et al., 2006; Hirata et al., 2008). For the entire dataset, different concentrations of pigments were recorded. The highest mean concentrations were for fucoxanthin present in all analysed samples, n=31, (0.17 mg m^{-3}) similarly to Tchl*b* (0.13 mg m^{-3}), n=31. The mean concentrations of other pigments were: 19'hex (n=28) – 0.08 mg m^{-3}, peri (n=14) – 0.06 mg m^{-3}, allo (n=31) – 0.04 mg m^{-3}, 19'but (n=26) – 0.02 mg m^{-3}, and zea (n=29) – 0.01 mg m^{-3}. Pigment concentration ranges varied by fjord (Figure 4). For example, peridinin concentrations in Isfjorden showed a the largest range of variability from 0.0015 to 0.20 mg m^{-3}. In Kongsfjorden, peridinin was identified in only two out of seven samples, but with a highly contrasting concentrations (0.002 mg m-3 and 0.157 mg m^{-3}). In Hornsund peridinin concentrations ranged from 0.024 to 0.046 mg m^{-3}. The smallest range of fucoxanthin concentration variability was recorded in Hornsund (from 0.018 to 0.236 mg m^{-3}) whereas wider ranges occurred in Kongsfjorden (from 0.026 to 0.650 mg m^{-3}) and Isfjorden (from 0.064 to 0.517 mg m^{-3}). For 19'but the highest concentrations occurred in Kongsfjorden and Isfjorden. 0.38 to 0.089 mg m^{-3}, while the lowest were in Hornsund (from 0.001 to 0.011 mg m^{-3}). 19'hex concentrations varied from 0.017 to 0.0245 mg m^{-3} in Kongsfjorden, from 0.039 to 0.96 mg m^{-3} in Isfjorden, and from 0.005 to 0.040 mg m^{-3} in Hornsund. The concentration of Tchl*b* varied from 0.051 to 0.377 mg m^{-3} in Isfjorden, from 0.032 to 0.235 mg m^{-3} in Kongsfjorden, and from 0.035 to 0.195 mg m^{-3} in Hornsund. Alloxanthin showed the greatest variability in Kongsfjorden, from 0.007 to 0.190 mg m^{-3}, while ranges in Hornsund and Isfjorden were narrower, from 0.008 to 0.044 mg m^{-3}, and from 0.006 to 0.054 mg m^{-3}, respectively. Zeaxanthin variability ranges were the largest in Isfjorden, from 0.005 to 0.050 mg m^{-3}, followed by Kongsfjorden (0.003 - 0.033 mg m^{-3}) and Hornsund (0.003 - 0.022 mg m^{-3}).

https://doi.org/10.5194/egusphere-2025-2800
Preprint. Discussion started: 28 August 2025

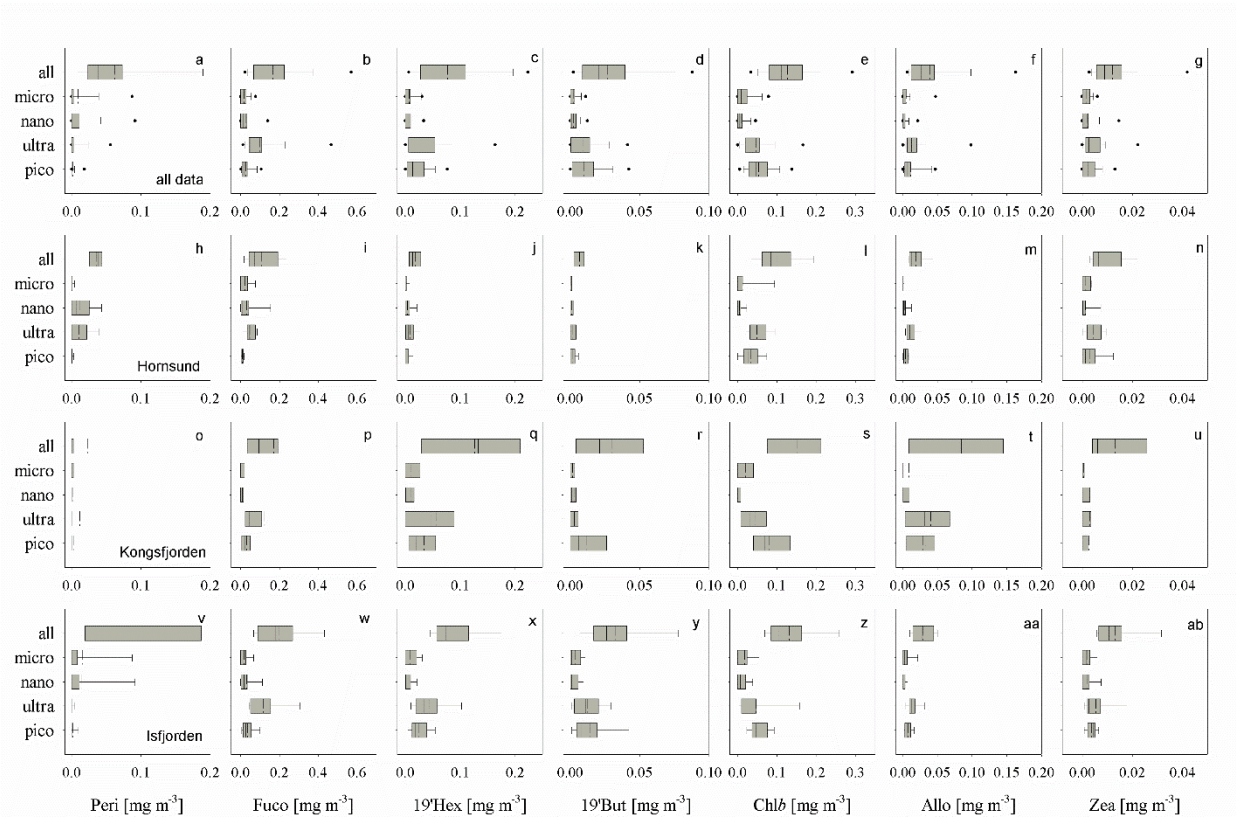

Figure 4: Ranges of variability of diagnostic pigments concentration (peridinine, fukoxantin, 19`hex-fukoxantin, 19`but-fukoxantin, chlorophyll *b*, alloxantin and zeaxantin) for the original water samples and in the size classes: micro, nano, ultra and pico for all dataset (a-g), and divided on sampling area: Hornsund (h-n), Kongsfjorden (o-u) and Isfjorden (v-ab). Boxes show the range from the 25th to the 75th percentile, whiskers between the 10th and 90th percentile. The straight line indicates the median, the dashed line the mean, and the dots show the minimum and maximum values.

3.3 Variability in the absorption properties of suspended and dissolved matter (total particles, detritus, phytoplankton, and CDOM)

Figure 5 presents the light absorption coefficient spectra for all suspended particles ($a_p(\lambda)$), detritus ($a_d(\lambda)$), and phytoplankton ($a_{ph}(\lambda)$) obtained from the analyzed dataset. The left panels (Figure 5a, c, e) illustrate the variability of these coefficients in the original, unfractionated seawater samples. The results indicate a variability of absorption coefficients exceeding an order of magnitude. At the selected wavelength of 443 nm, the observed ranges of variability of the $a_p(443)$, $a_d(443)$ and $a_{ph}(443)$ coefficients for the entire data were as follows: 0.078 – 1.49 m^{-1}, 0.063 – 1.22 m^{-1}, and 0.042 – 0.203 m^{-1}, respectively. The largest range of variability was observed in Hornsund, where the mean values of $a_p(443)$, $a_d(443)$ and $a_{ph}(443)$ were 0.459 ± 0.407 m^{-1}, 0.376 ± 0.347 m^{-1}, 0.077 ± 0.047 m^{-1}, respectively. In Kongsfjorden and Isfjorden the mean values of $a_p(443)$,

https://doi.org/10.5194/egusphere-2025-2800
Preprint. Discussion started: 28 August 2025

$a_d(443)$ and $a_{ph}(443)$ were lower: 0.174 ± 0.042 m^{-1} and 0.186 ± 0.104 m^{-1}, 0.108 ± 0.047 m^{-1} and 0.127 ± 0.098 m^{-1}, 0.067 ± 0.028 m^{-1} and 0.060 ± 0.020 m^{-1}. The right panels in Figure 5 (b, d, f) show the variability of $a_p(\lambda)$, $a_d(\lambda)$ and $a_{ph}(\lambda)$, calculated for micro-, nano-, ultra- and pico-particles. Bold lines indicate the mean spectra in a given size class, while thin dashed lines show the range of variability (min-max). The variability excided one order of magnitude.

Figure 5g presents the light absorption coefficient spectra of chromophoric dissolved organic matter (CDOM derived from the analyzed dataset. For the total data, $a_{CDOM}(443)$ varied from 0.010 m^{-1} to 0.164 m^{-1} with a greater variability observed again in Hornsund. The average spectral slope coefficient ($S_{300-600}$) was 0.0186 ± 0.003 m^{-1}, with regional differences: In Hornsund $S_{300-600}$ was 0.0185 ± 0.0049 m^{-1}, in Kongsfjorden 0.0176 ± 0.0014 m^{-1}, and 0.0194 ± 0.0011 m^{-1} in Isfjorden.

Based on the light absorption coefficients: $a_{ph}(\lambda)$, $a_d(\lambda)$ and $a_{CDOM}(\lambda)$, the light absorption budget at 443 nm was calculated (Figure 5h). In the analyzed data set, the average contribution to the total light absorption at 443 nm was: phytoplankton - 28% ± 13% (Table 3), ,CDOM - 17% ± 8%, and detritus - 55% ± 17%, indicating that detritus was the dominant light absorbing component. When considering regional differences, in Hornsund the average contributions were: of $a_{ph}(443)$ - 18% ± 11%, of $a_d(443)$ - 69% ± 17%, and of $a_{CDOM}(443)$ - 12% ± 10%. In Kongsfjorden the average proportions were: of $a_{ph}(443)$ - 32% ± 14%,, $a_d(443)$ - 48% ± 17%, and $a_{CDOM}(443)$ -20% ± 5%. In Isfjorden, the average contributions were: $a_{ph}(443)$ - 32% ± 1%, $a_d(443)$ - 50% ± 13% and $a_{CDOM}(443)$ - 18% ± 5%.

https://doi.org/10.5194/egusphere-2025-2800
Preprint. Discussion started: 28 August 2025

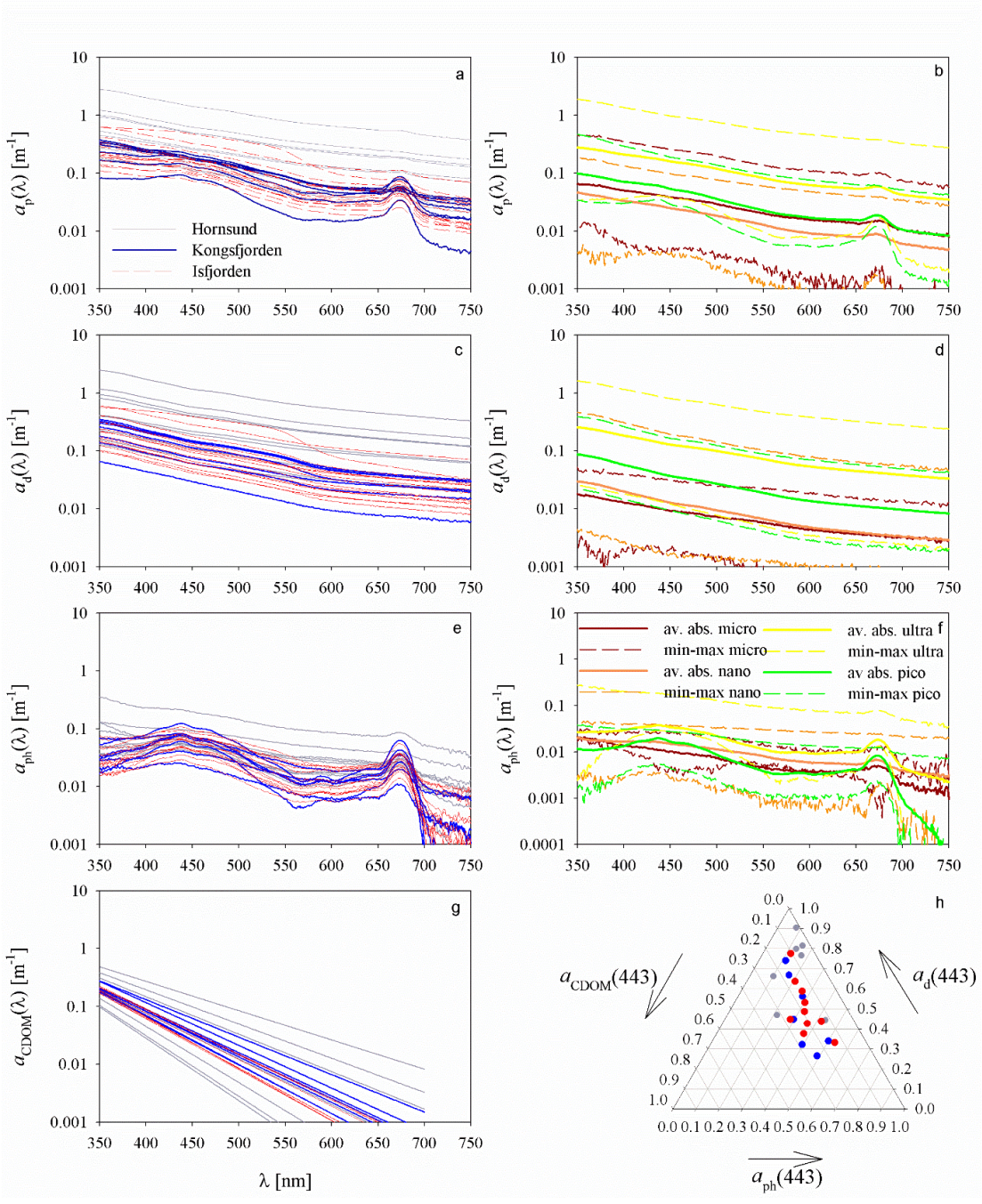

330 **Figure 5: Spectra of light absorption coefficients for suspended particles in seawater ($a_p(\lambda)$), detritus ($a_d(\lambda)$) and phytoplankton ($a_{ph}(\lambda)$) in original, unfractionated samples (left panels: a, c, e) and for micro-, nano-, ultra-, and pico-size classes (right panels: b, d, f). Panel (g) shows the spectra of CDOM absorption coefficients ($a_{CDOM}(\lambda)$), while panel (h) presents a ternary plot of the absorption budget at 443 nm for the analyzed dataset.**

https://doi.org/10.5194/egusphere-2025-2800
Preprint. Discussion started: 28 August 2025

Table 3: Absorption budget at 443 nm (n=38). Mean ± SD and ranges are shown for the entire dataset and by sampling area.

	all data	Hornsund	Kongsfjorden	Isfjorden
$a_{ph}(443)/a(443)$	28.1 % ± 13.4 %	18.4 % ± 11.1 %	32.1 % ± 13.9 %	32.0 % ± 0.8 %
	7.90 % -53.2 %	7.90 % - 43.6 %	11.6 % - 50.1 %	12.1 % - 53.2 %
$a_d(443)/a(443)$	55.1 % ± 17.7 %	69.3 % ± 16.5 %	47.7 % ± 17.0 %	50.2 % ± 12.6 %
	26.4 % - 90.4 %	44.2 % - 90.4 %	26.4 % - 74.0 %	33.1 % - 77.4 %
$a_{CDOM}(443)/a(443)$	16.9 % ± 7.7 %	12.3 % ± 10.4 %	20.3 % ± 5.3 %	17.7 % ± 4.9 %
	1.7 % - 31.8 %	1.7 % - 31.8 %	14.4 % - 28.3 %	10.5 % - 27.1 %

3. 4 Contribution of particle size classes to total light absorption by all particles, detritus, and phytoplankton at 443 nm

Analysis of the light absorption coefficients $a_p(443)$, $a_d(443)$ and $a_{ph}(443)$, allowed the determination of the contribution of individual particle size classes to the total light absorption coefficients. Table 4 shows the results for the whole dataset and for Hornsund, Kongsfjorden, and Isfjorden, based on the classification of Ciotti et al. (2002). Across all cases, ultra-particles contributed the most to the total absorption of light accounting for over 44%. Pico-particles contributed on average about 25%, nano-particles accounted for about 10% for $a_p(443)$ and $a_d(443)$ and 19% for $a_{ph}(443)$. Micro-particles had the smallest contribution in the absorption of light, on average about 4-9%. The distribution of the contribution of the individual size classes to the total light absorption is illustrated in Figure 6, taking into account the division into the sampling areas: Hornsund, Kongsfjorden and Isfjorden. In Hornsund, the average contribution to $a_p(443)$ was 3.4%, for micro-particles 12.5% for nano-particles, 62% for ultra-particles, and 22% for pico-particles. In Kongsfjorden, the average contribution to $a_p(443)$ was for micro-particles: 4.3%, nano-particles: 6.2%, ultra-particles: 61% and pico-particles: 28.5%, respectively. In the case of Isfjorden, the average proportion in $a_p(443)$ of particles from the micro, nano, ultra and pico size classes was 5.2%, 11.6%, 55.3% and 28%, respectively (Figure 6a). In the case of micro-particles the lowest contribution to $a_d(443)$, was recorded in Hornsund (average 1.2%), while in Kongsfjorden and Isfjorden it was 4.6% and 5.4%, respectively. The proportion of nano-particles in $a_d(443)$ was higher and averaged 12% in Horsund, 7.8% in Kongsfjorden and 10.7% in Isfjorden. In all study areas, ultra-particles dominated the total $a_d(443)$ accounting on average for 65% in Hornsund, 63% in Kongsfjorden and 60% in Isfjorden. Pico-particles also contributed significantly: 22% in Hornsund, 25% in Kongsfjorden and 24% in Isfjorden (Figure 6b). More pronounced regional variation was observed in the contribution of different sizes classes to the absorption of light by phytoplankton (Figure 6c). The smallest contributions of micro-particles were observed in Hornsund (7.2%) and in Isfjorden (7.6%), with a slightly higher share in Kongsfjorden (12.6%). Nano-particles had the largest contribution to $a_{ph}(443)$ in Hornsund (26%) and Isfjorden (21%) and the least in Kongsfjorden (6.1%). Among all size classes, ultra-particles had the largest share in $a_{ph}(443)$: in Hornsund - 46.4%, in Kongsfjorden - 51% and in Isfjorden - 39%. Pico-particles accounted for 20.5% in Hornsund, while their average share in Kongsfjorden and Isfjorden was aproximatelly 31%.

https://doi.org/10.5194/egusphere-2025-2800
Preprint. Discussion started: 28 August 2025

Table 4: Contributions of particle size classes (micro, nano, ultra, pico) to total light absorption by particles, detritus, and phytoplankton at 443 nm (n=38). Mean ± SD and ranges are provided for all samples and by sampling area.

	all data	Hornsund	Kongsfjorden	Isfjorden
$a_{p,micro}/a_p$	4.5 % ± 6.2 %	3.4 % ± 5.7 %	4.3 % ± 5.8 %	5.2 % ± 6.6 %
	0-23%	0-18.3%	0-13.9 %	0-23 %
$a_{p,nano}/a_p$	10.6 % ± 8.5 %	12.5 % ± 9.9 %	6.2 % ± 4 %	11.6 % ± 8.5 %
	0-31.6 %	0-30 %	2 % - 14.9 %	0- 31.6 %
$a_{p,ultra}/a_p$	58.5 % ± 11.1 %	61.9 % ± 115 %	61 % ± 9.6 %	55.3 % ± 10.5 %
	35.7 %-75.5 %	44 %-73.7 %	44.4 % - 75.5 %	35.7 % -73.4 %
$a_{p,pico}/a_p$	26.4 % ± 8.4 %	22.2 % ± 6.2 %	28.5 % ± 8 %	28 % ± 8.7 %
	13.5 %-43.3 %	13.5 % - 30.5 %	18.3 % - 40.4 %	15.9 % - 43.3 %
$a_{d,micro}/a_d$	4 % ± 6.6 %	1.2 % ± 1.9 %	4.6 % ± 7.5 %	5.4 % ± 7.4 %
	0-24.5 %	0-5.3 %	0-21.7 %	0-24.5 %
$a_{d,nano}/a_d$	10.4 % ± 9.4 %	11.9% ± 12.4 %	7.8 % ± 4.7 %	10.7 % ± 8.7 %
	0-33.1 %	0– 33.1 %	0.3 % - 16.5 %	0- 29.3 %
$a_{d,ultra}/a_d$	62 % ± 11.9 %	64.7 % ± 11.3 %	62.7 % ± 11.2 %	59.9 % ± 12.1 %
	41.2 %-84.4 %	43.3 % - 77.1 %	41.2 % - 74.2 %	41.5 % - 84.4 %
$a_{d,pico}/a_d$	23.7 % ± 7.1 %	22.1 % ± 6.8 %	24.8 % ± 5.8 %	24 % ± 7.6 %
	11.7 %-39.5 %	14.3 % - 36.9 %	16.1 % - 31.8 %	11.7 % - 39.5 %
$a_{ph,micro}/a_{ph}$	8.6 % ± 15.9 %	7.2 % ± 10.6 %	12.6 % ± 25 %	7.6 % ± 12.3 %
	0-73.4 %	0-26 %	0-73.4 %	0-40 %
$a_{ph,nano}/a_{ph}$	19.1.% ± 21.8 %	25.9% ± 21.5 %	6.1 % ± 6.9 %	21 % ± 23.9 %
	0-79.9%	0-79.9 %	0 – 21.2 %	0- 78.7 %
$a_{ph,ultra}/a_{ph}$	44 % ± 19.8 %	46.4 % ± 21.1 %	51.1 % ± 23.5 %	39.3 % ± 15.3 %
	0 -87.2 %	13.1 % - 87.2 %	0 – 75.2 %	0.24 %-64.7 %
$a_{ph,pico}/a_{ph}$	28.3 % ± 12.9 %	20.5 % ± 10.2 %	30.1 % ± 10.5 %	32.1 % ± 13.3 %
	0-51.3 %	7 % - 40.2 %	17.1 % - 47.7 %	0- 51.3%

https://doi.org/10.5194/egusphere-2025-2800
Preprint. Discussion started: 28 August 2025

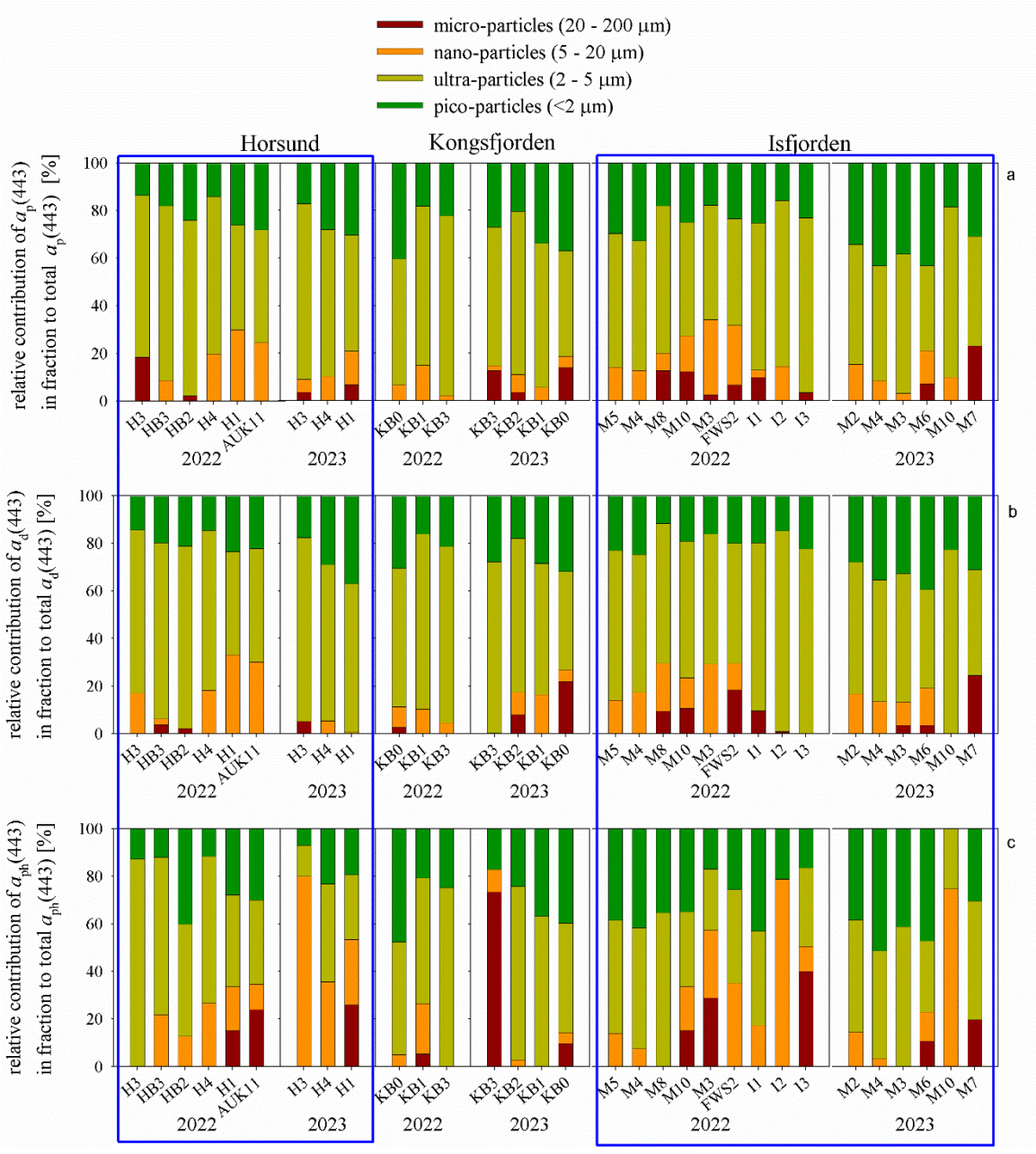

Figure 6: Relative contribution of particle size classes to total light absorption by all particles (a), detritus (b), and phytoplankton (c), based on the four-class division of Ciotti et al. (2002): micro-, nano-, ultra-, and pico-particles in Hornsund, Kongsfjorden and Isfjorden in summer 2022 and 2023

https://doi.org/10.5194/egusphere-2025-2800
Preprint. Discussion started: 28 August 2025

4 Discussion

We present the results of analyses of the variability in concentrations of SPM (including POM and PIM fractions), Tchl*a* and absorption properties of suspended particles for 4 size classes in the waters of three selected fjords in western Spitsbergen. So far, studies considering particles size classes in such detail, have been rare. Examples include the work of Meler et al. (2023) for the waters of the southern Baltic Sea region and Woźniak et al. (2024b) for the western Spitsbergen fjords. Previous studies on the fractionation of suspended particles by particle size in the water column focused mainly on the analysis of their chemical composition within the GEOTRACE projects (Lam et al., 2015, 2018; Yigiterhan et al., 2020) using two size classes (<50 µm and >50 µm), or on optical properties of SPM size fractions in narrower size ranges (0.2-0.4 µm, 0.4-0.7 µm, 0.7-10 µm and > 10 µm) as in Mohammadpour et al. (2017).

4.1 Composition of SPM in original and fractionated samples

In our dataset, the range of SPM variability was from 0.56 g m^{-3} to 12.14 g m^{-3} (mean 2.47 g m^{-3}), and PIM from 0.12 g m^{-3} to 10.01 g m^{-3} (mean 1.84 g m^{-3}). Woźniak et al. (2024b) reported a wider range from 0.8 g m^{-3} to 25.2 g m^{-3}, of SPM variability for the same area which was related to the fact that the measuring stations were located closer to the glaciers. In a broader dataset from the same study area, Woźniak et al. (2024a) recorded an even larger range of SPM concentrations, from 0.66 g m^{-3} to 213 g m^{-3}, with PIM from 0.28 g m^{-3} to 199 g m^{-3}. High SPM and PIM occur near melting glaciers or at river mouths. Dragańska-Deja (2024) documented high glacial SPM in Hornsund and Konsfjorden (in the summer of 2016-2018) with variability from 16.7 g m^{-3} to 71.7 g m^{-3} and PIM from 14.38 g m^{-3} to 68.22 g m^{-3}. Similar values were found in Isfjorden by Szeligowska et al. (2021), where the variability of SPM and PIM observed in the surface layer in July 2019 closely matched the dataset analyzed by us. Comparable SPM variability was observed in Kongsfjorden, while in Hornsund it was characterized by the highest SPM variability. It should be noted here that particle size fractionation in the analyzed data set was not conducted at stations with particularly high concentrations of suspended particles due to time and economic constrains. In contrast studies by Woźniak et al. (2024a) and Dragańska-Deja (2024) focused more on areas located closer to glacial fronts. Halbach et al. (2019) documented higher SPM concentrations in Kongsfjorden during turn of July and August 2017 (i.e. a similar study period as ours), with values ranging from 8.8 g m^{-3} to 95.8 g m^{-3}. Similarly, Son and Kim (2018) reported SPM concentrations ranging from 0.25 g m^{-3} to 10.5 g m^{-3} in Kongsfjorden and Krossfjorden in the years 2006-2008.These elevated SPM concentrations likely resulted from meltwater discharge carrying sediments from the calving of tidal glaciers (Svendsen et al., 2002). In Kongsjorden, the primary source of suspended particles is Kronebreen glacier followed by other three glaciers: Kongsvegen, Kongsbreen and Conwaybreen. The most intensive calving of the glaciers typically occurs in July, and gradually slows in August (Schellenberger et al., 2015).

Isfjorden is the largest fjord system of Spitsbergen (Nilsen et al.; 2008), with freshwater input mainly from glacial calving and ablation from the surrounding glaciers, located mainly on the northern side of the fjord. Hornsund is influenced by several glaciers and the inflow of cold waters carried by the Sørkapp Current (Błaszczyk et al., 2013, 2019).

https://doi.org/10.5194/egusphere-2025-2800
Preprint. Discussion started: 28 August 2025

In comparison, significantly lower mean concentrations of SPM and PIM were recorded in the Norwegian fjords Sognefjord and Trondheimsfjord by Mascarenhas et al. (2017), averaging around. 1.20 g m^{-3} and 0.60 g m^{-3}, respectively. Sognefjord is the longest and deepest fjord in Norway (over 200 km and 1300 m deep). The inner end of the Sognefjord is covered by the largest glacier in Europe (Jostedalsbreen), which causes large amounts of cold glacier meltwater carrying large suspended solids loads to flow into the fjord waters. Approximately 11 rivers also flow into the fjord, contributing to a substantial w inflow of fresh water, that carries CDOM and suspended matter, thereby affecting the transparency of the water. Trondheimsfjord, a bay of the Norwegian Sea, is the third longest fjord in Norway (130 km long). Six rivers flow into the fjord. The fjord is characterized by rich marine life (about 90 species of fish) and the largest biological production among Norwegian fjords. In turn, in the fjords of Greenland (Uummannaq Fjord, Vaigat-Disco Bay and Gogthabsfjord), Holinde and Zielinski (2016) and Mascarenhas and Zielinski (2019) observed similar SPM and PIM variability during the summer seasons of 2012 and 2017 as in the dataset analyzed by us. Like the fjords of Spitsbergen, Greenland fjords are strongly influenced by glacial meltwater. Uummannaq Fjord, located on the west coast of Greenland, is a mixing zone for meltwater from glaciers and ocean water from Baffin Bay. Just to the south lies Vaigat Disco Bay, an open system receiving water from three glaciers. Disco Bay is a semi-enclosed region influenced by the subarctic waters of southwestern Greenland and the arctic waters from Baffin Bay. Godthabsfjord is a subarctic fjord with many branches, located on the southwestern coast of Greenland. The inner part of the fjord is connected to 3 glaciers, that supply large volumes of meltwater and ice to the fjord waters.

In the analyzed data set, inorganic particles dominated, as indicated by the POM/SPM ratio of 33% in the original samples (Figure 3). In the studies of Woźniak et al. (2024a and b), in the summer seasons of 2021-2022, the average POM/SPM ratios were 25% and 27%, respectively, suggesting an even greater dominance of the inorganic fraction of the suspended matter in the region, especially near the glaciers. The dominance of PIM results mainly from the inflow of suspended matter from rivers and melting glaciers to the sea waters (Cottier et al., 2005; Darlington, 2015; Błaszczyk et al., 2019; Dragańska-Deja, 2024). In contrast, Mascarenhas et al. (2017) documented higher mean POM/SPM ratios of aproximately 50% in the Norwegian fjords of Sognefjord and Trondheimsfjord. Similarly, Mascarenhas and Zielinski (2019) reported comparable values of mean POM/SPM in the Greenlandic fjords of Vaigat-Disco Bay and Gogthabsfjord. This suggests that in the Norwegian and Greenland fjords, the share of organic and inorganic particles in suspended matter was similar, without a clear dominance of one fraction. For comparison, in a completely different marine system (however, also in the case of optically complex waters, for which similar analyses were carried out for size fractions as in this work), i.e. for the Baltic Sea waters, Meler et al. (2023) obtained an average POM/SPM ratio of 53% for all data, which indicates the predominance of organic matter in the total SPM. The analysis of SPM distribution across size classes (micro-, nano-, ultra- and pico-) in our dataset (Figure 2 a) revealed average distribution of 16%, 14%, 50% and 19%, respectively. A similar distribution was obtained by Woźniak et al. (2024b) for the dataset collected closer to the glacial fronts, where the combined share of micro- and nano-particles was 28%, ultra-particles 53% and pico-particles 19%. In the Baltic Sea, Meler et al. (2023) noted greater variability in the distribution of SPM size fractions. As in our study, micro-particles had the lowest average contribution (17%). On the other hand, the proportions of the remaining size classes in SPM were more evenly distributed, each on average about 27%. These findings suggest that

https://doi.org/10.5194/egusphere-2025-2800
Preprint. Discussion started: 28 August 2025

the composition of particle size fractions in Arctic fjords and the Baltic Sea differs significantly. The proportion of micro-particles (16% in the analyzed data set and 17% in the Baltic Sea) in SPM is similar in both water bodies, but the proportions of other particle size classes are more diverse. In fjords, ultra-particles dominate, followed by a large contribution of pico-
435 particles, while in the Baltic Sea there is no visible dominance of particle size classes and the proportions of these classes is similar for the entire data set.

Figure 7 shows the relationships between the contributions of individual size classes in SPM to the total SPM in relation to the content of organic matter POM in the total SPM. Despite the low value of the determination coefficient R^2<0.4, a trend is visible indicating that with the increase of POM/SPM the proportions of micro and pico size classes in the total SPM increase,
440 while the proportions of nano and ultra size classes in the total SPM decrease. Our results are similar or close to those obtained by Woźniak et al. (2024b).

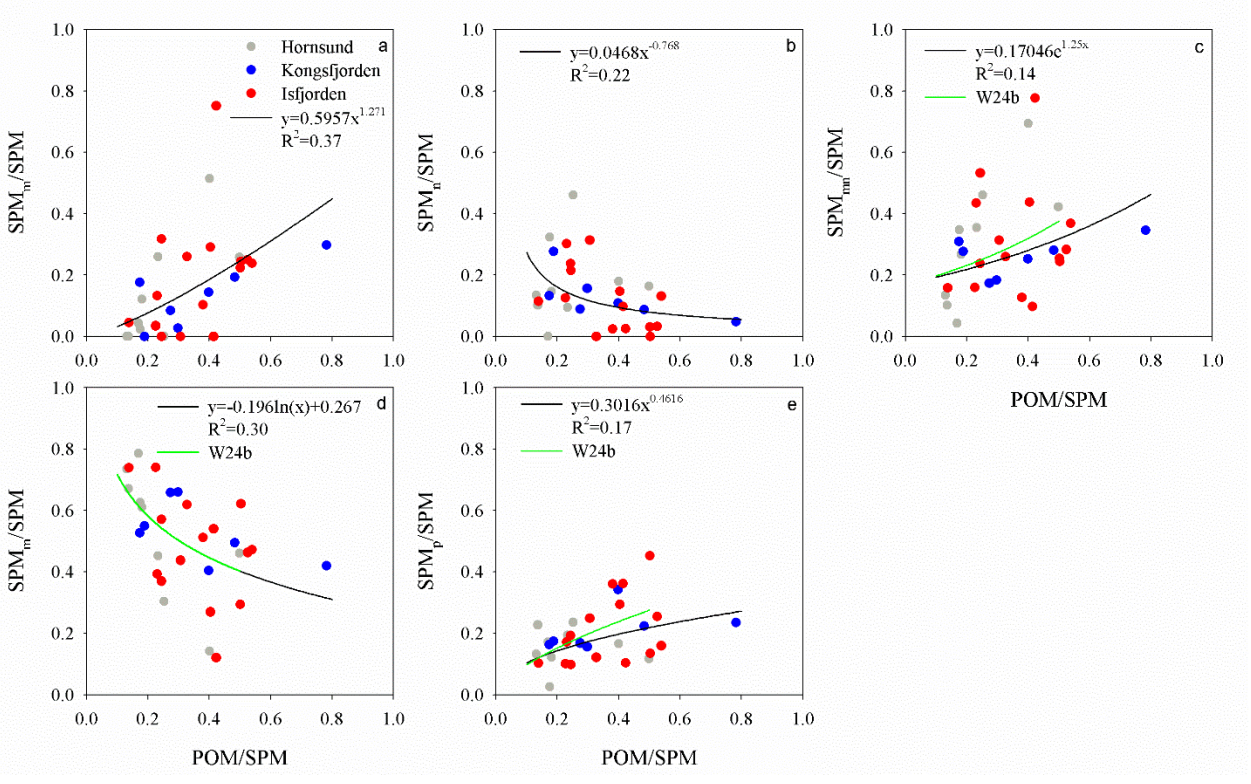

Figure 7: Relationships between selected parameters describing the composition of suspended particulate matter (SPM) and its fractions: (a) SPM_m/SPM vs. POM/SPM; (b) SPM_n/SPM vs. POM/SPM; (c) SPM_{mn}/SPM vs.
445 **POM/SPM; (d) SPM^u/SPM vs. POM/SPM; (e) SPM_p/SPM vs. POM/SPM. Indexes m, n, mn, u, and p denote micro-, nano-, micro+nano, ultra-, and pico-particles, respectively. Black lines show the best-fit regressions, while W24b indicates the approximation proposed by Woźniak et al. (2024b).**

https://doi.org/10.5194/egusphere-2025-2800
Preprint. Discussion started: 28 August 2025

4.2 Composition of Tchl*a* in original samples and size fractions

The range of variability of Tchl*a* concentration, a key indicator of phytoplankton biomass, in the analyzed set for unfractionated (original) data was smaller than that of SPM and ranged from 0.27 mg m^{-3} to 3.20 mg m^{-3}. Similar ranges of variability were reported by Woźniak et al. (2024a and b). The largest was observed in Kongsfjorden and it overlapped with the range for the whole dataset, followed by Isfjorden (0.46 g m^{-3} - 2.15 g m^{-3}), and the smallest range of variability in Hornsund (0.27 g m^{-3} - 1.54 g m^{-3}). In contrast, Son and Kim (2018) in Kongsfjorden and Krosfjorden and Halbach et al. (2019) in Kongsfjorden, recorded approximately two fold higher ranges in comparable month, ranging from 0.03 g m^{-3} to about 7 g m^{-3} and from 0.2 g m^{-3} to 7.4 g m^{-3}, respectively. These broader ranges of variability likely reflect interannual differences in glacier melt intensity, which is dependent on atmospheric conditions (temperature, pressure, insolation and the influence of warm air masses). Increased glacier melting results in bigger nutrients availability in the fjord waters, which in turn increases phytoplankton productivity. The average Tchl*a* concentrations in the Norwegian fjords (Sognefjord and Trondheimsfjord, Mascarenhas et al., 2017) was comparable to those in Kongsfjorden, but approximately twice as high as those in Hornsud or Isfjorden. In turn, the Greenland fjords were characterized by similar ranges of Tchl*a* variability as the analyzed dataset (Holinde and Zielinski, 2016; Mascarenhas and Zielinski, 2019).

Our analyses included the distribution of Tchl*a* across different size classes (micro-, nano-, ultra- and pico-) to the total Tchl*a* for the total data and divided into fjords: Hornsund, Kongsfjorden, Isfjorden. The Tchl*a* proportions obtained by us in the size classes for the total data (Figure 2d) were on average: micro-12%, nano- 12%, ultra- 47% and pico- 29%, respectively. These results are similar to those obtained by Woźniak et al. (2024b), where the proportion of micro + nano-particles was on average 20%, and ultra-particles accounted for 52%. These proportions are different from those observed in the Baltic Sea waters (Meler et al., 2023), where the contribution of ultra-particles and pico-particles in Tchl*a* were similar, on average 35%. Also the contributions of micro- and nano-particles were higher than in the Spitsbergen fjords, on average 16% and 18%. In the Atlantic Ocean waters, the total Tchl*a* was dominated by picoplankton (61%), followed by nano- and ultraplankton combined (29%), with the smallest proportion of microplankton (9%) (Maranon et al., 2001). In the Strait of Magellan, where the Atlantic and Pacific Oceans mix, micro-, nano-, and ultra-particles dominated in spring (88%), and pico-particles had a contribution of 12%. In summer, the contribution of pico-particles increased to 60%. However, at the turn of summer and autumn, the contribution of pico-particles decreased to 47% (Decembrini et al., 2014).

4.3 Variability of light absorption coefficients and absorption budget

The light absorption coefficients of particles and CDOM depend on the composition of suspended particles, dissolved organic substances, and phytoplankton pigments. In the analyzed dataset, the average values for $a_p(443)$, $a_d(443)$, $a_{ph}(443)$ and $a_{CDOM}(443)$ were 0.26 m^{-1}, 0.20 m^{-1}, 0.07 m^{-1} and 0.06 m^{-1}, respectively. Compared to the Baltic Sea (Meler et al,. 2023), the $a_p(443)$, $a_{ph}(443)$ and $a_{CDOM}(443)$ values in our dataset were lower (by factor of 0.8, 0.33, and 0.24, respectively), while $a_d(443)$ was almost 2 times higher. While both fjord waters and Baltic waters are optically complex and significantly influenced by

https://doi.org/10.5194/egusphere-2025-2800
Preprint. Discussion started: 28 August 2025

terrestrial inputs, key differences exist. Fjord waters are dominated by inorganic and mineral suspensions, while in the Baltic Sea, especially in the coastal zone, CDOM and phytoplankton dominate the absorption budget. The lowest mean values of $a_p(443)$ were observed in Kongsfjord (0.17 m^{-1}) and Isfjorden (0.19 m^{-1}), while in Hornsund the mean $a_p(443)$ was more than 2.5 times higher (0.46 m^{-1}). Similar trends in mean values can be seen for $a_d(443)$ and $a_{ph}(443)$: lower mean values in Kongsfjorden and Isfjorden ($a_d(443)$ equal to 0.10 m^{-1} and 0.12 m^{-1} and $a_{ph}(443)$ equal to 0.07 m^{-1} and 0.06 m^{-1}), and higher in Hornsund ($a_d(443)$ = 0.38 m^{-1} and $a_{ph}(443)$ = 0.08 m^{-1}).

The contribution of individual seawater components in the total light absorption for the analyzed data set from the turn of July and August is shown in Figure 5h. For the wavelength of 443 nm, the largest contribution in absorption had detritus (55%), followed by phytoplankton (28%) and CDOM (17%). Similar proportions were noted by Matsuoka et al. (2011) for the Western Arctic Shelf Basin. Son and Kim (2018) in August in Kongsfjorden and Krossfjorden, also found the dominance of detritus in light absorption (51%), though CDOM contributed more (33%) and phytoplankton less (16%). In contrast, in June, CDOM dominated (50-64%), followed by detritus (15-28%) and phytoplankton (21%). Seasonal variability of the proportions of CDOM, detritus and phytoplankton in the fjords is related to the atmospheric, biological and hydrological conditions in the region, which also affect the melting of glaciers, causing the supply of variable amounts of nutrients, minerals, inorganic elements suspended and dissolved in water to the fjord waters. In Norwegian fjords, Macsarenhas et al. (2017) showed an even greater dominance of CDOM in light absorption (> 60%) (likely due to increased river runoff and glacier melting), with lover contribution from phytoplankton (> 20%) and detritus (5-10%). In contrast, Baltic Sea waters (for a data set from different months of the year), showed the following average absorptions contributions CDOM - 52%,, phytoplankton - 29% and detritus 19% in the total light absorption.

4.3 Light absorption variability vs Tchl*a* and SPM

Figure 8 shows the values of the absorption coefficients $a_p(443)$ as a function of Tchl*a* and SPM concentrations, for both original seawater samples and for the micro-, nano-, ultra-, and pico-particle size classes. The data were divided by sampling location. The obtained approximation curves are shown in the power form ($y=Ax^B$), only in cases where the coefficient of determination, R^2, was greater than 0.1. It can be seen that both for the total number of particles and for the size classes there is no visible dependence of $a_p(443)$ on Tchl*a*. A notable exception is micro-particles, where a strong dependence of $a_p(443)$ on Tchl*a* is found (R^2= 0.88). Differences between individual fjords are also visible. Samples from Hornsund are characterized by higher values of $a_p(443)$ coefficients and simultaneously lower Tchl*a* concentrations. The particles in Hornsund were more dominated by mineral particles than in the case of Kongsfjorden and Isfjorden, which receive more organic particles. Analyzing $a_p(443)$ from SPM, dependencies were determined for all particles and for size classes excluding the micro-particle class. These dependencies were characterized by R^2 coefficients, respectively: for all particles – 0.77, nano-particles – 0.20, ultra-particles – 0.87, and pico-particles – 0.35. The results obtained here can be compared with literature data, in particular with the work of Meler et al. (2023), who conducted similar analyses for the Baltic Sea (also included in Figure 8). It can be seen that the relations of $a_p(443)$ on chlorophyll *a* concentrations obtained for the Baltic Sea differ significantly from our dataset,

https://doi.org/10.5194/egusphere-2025-2800
Preprint. Discussion started: 28 August 2025

which is dominated by inorganic particles and thus is not correlated with Tchl*a*. In contrast, the $a_p(443)$ on SPM correlations are more comparable between regions, particularly for total absorption and to a lesser extent, ultra-, pico-, and micro-particles. However, for nano-particles, the approximation does not align. For the relationship of the light absorption coefficients of the total particles on the chlorophyll *a* concentrations, two more approximations obtained by Mascarenhas and Zielinski (2018) for Norwegian fjords were compared (Figure 8a). It can be seen that both lines fall below our data set, which indicates a completely different nature of the variability of the absorption coefficients of particles relative to Tchl*a* in those fjords.

Figure 9 shows the values of the absorption coefficients $a_d(443)$ as a function of Tchl*a* and SPM concentrations, for both the original seawater samples each particle size class. The approximations are also presented as a power function. Similarly to the relationship of $a_p(443)$ vs Tchl*a*, the dependence of $a_d(443)$ vs Tchl*a* also does not indicate any visible correlations, neither for the total particle pool nor within the size classes. This is due to the dominance of inorganic and mineral particles. The approximations of $a_d(443)$ vs SPM were determined for total particles and most size classes, except for micro-particles. The R^2 values are: for total particles – 0.79, for nano-particles – 0.13, for ultra-particles – 0.90 and for pico-particles – 0.47, respectively. Figure 9a shows the fit obtained by Son and Kim (2018) for Kongsfjorden and Korossfjorden and has similar coefficient values to our approximation (not shown in the figure), whose R^2 coefficient was very low < 0.1. In turn, the Tchl*a* approximations obtained for the Baltic Sea (Meler et al., 2023) do not align with our observations, which results from the different composition of the suspended matter in the Baltic Sea, where organic detritus dominates, while in the Spitsbergen fjords mineral particles prevail. In turn, the relationships of $a_d(443)$ vs SPM obtained by Meler et al. (2023) for the Baltic Sea for total detritus particles and pico-particles differ slightly, but for nano-particles and ultra-particles a significantly different slope of the curves is visible. For micro-particles, the approximation of Meler et al. (2023) does not completely coincide with our observations for the Spitsbergen fjords.

Figure 10 shows the relationships of the $a_{ph}(443)$ as a function of Tchl*a* and SPM concentrations for both the original water samples and the particle size classes. The approximation of $a_{ph}(443)$ vs Tchl*a* in the form of power functions show moderate correlations for the total particles ($R^2 = 0.40$) and the pico-particles ($R^2 = 0.48$), which is consistent with the inorganic particles dominated in our dataset. The relations of $a_{ph}(443)$ vs SPM shows weaker correlations for all particles $R^2 = 0.14$, micro-particles $R^2 = 0.57$ and nano-particles $R^2 = 0.32$. Figure 10a compares our $a_{ph}(443)$ vs Tchl*a* data with previously published relationships for Arctic and fjords waters (Mascarenhas and Zielinski, 2018; Son and Kim, 2018; Tripathy et al., 2021; Woźniak et al., 2024a), Atlantic waters (Devred et al., 2022), and the Baltic Sea (Meler et al., 2023). It can be seen that the relationships obtained by Tripathy et al. (2021) most closely matches our results. The relationships from Woźniak et al. (2024a), Devred et al. (2022), and Son and Kim (2018) fall below our dataset, while those by Mascarenhas and Zielinski (2018) and Meler et al. (2023) are characterized by different slopes of the curves. The analysis of the dependence of $a_{ph}(443)$ vs SPM shows significant differences between our data and Baltic Sea approximations, underscoring the importance of particle composition in determining optical properties in different marine environments.

https://doi.org/10.5194/egusphere-2025-2800
Preprint. Discussion started: 28 August 2025

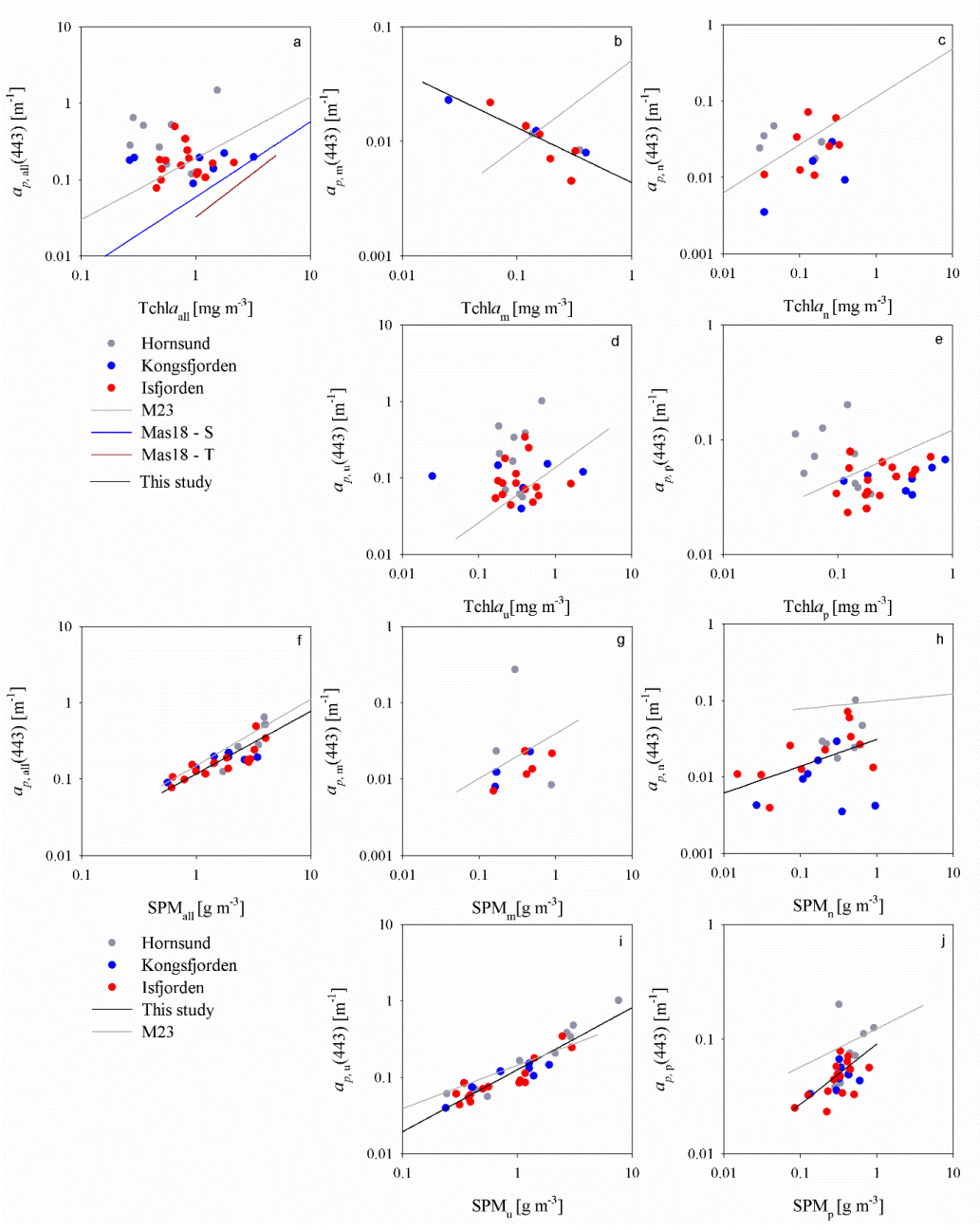

545

Figure 8: Relationships between absorption coefficients at 443 nm and Tchl*a* (a-e) or SPM (f-j) by all unfractionated particles (a, f) and in size classes: micro (b, g), nano (c, h), ultra (d, i) and pico (e, j). The black lines indicates the relationships obtained in this study, the gray lines (M23) the relationship in Meler et al. (2023) for the Baltic Sea. The blue (Mas18-T) and red lines (Mas18-T) show the relationships for Norwegian fjords: S - Sognefjord, T – Trondheimsfjord, of Mascarenhas et al. (2018).

550

https://doi.org/10.5194/egusphere-2025-2800
Preprint. Discussion started: 28 August 2025

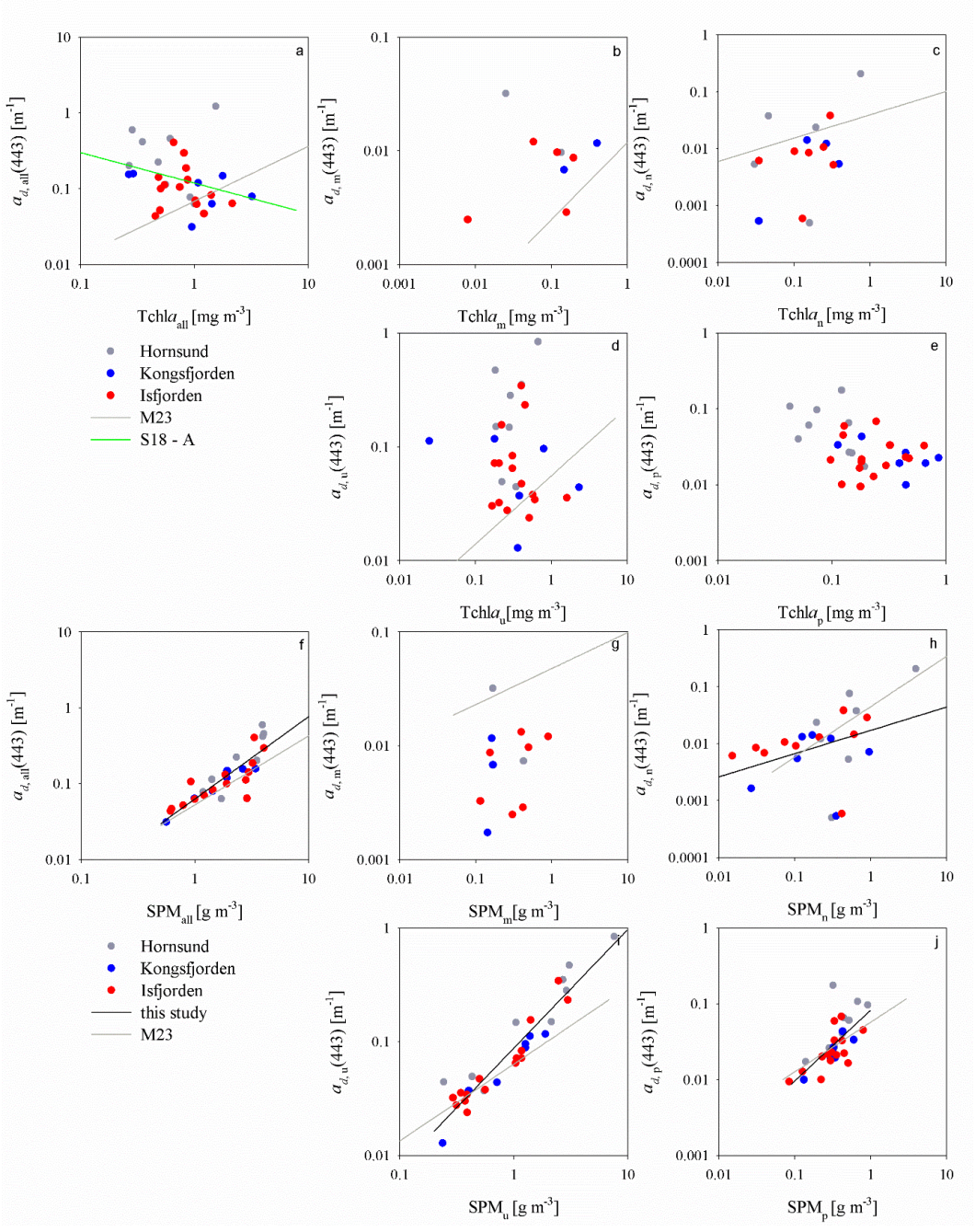

Figure 9: Relationships between absorption coefficients at 443 nm and Tchl*a* (a-e) or SPM (f-j) by all unfractionated detritus (a, f) and in size classes: micro (b, g), nano (c, h), ultra (d, i) and pico (e, j). The black lines indicates the relationships obtained in this study, M23 the relationship in Meler et al. (2023) for the Baltic Sea. S18 show the relationship for Kongsfjorden and Krossfjorden in Son and Kim (2018).

https://doi.org/10.5194/egusphere-2025-2800
Preprint. Discussion started: 28 August 2025

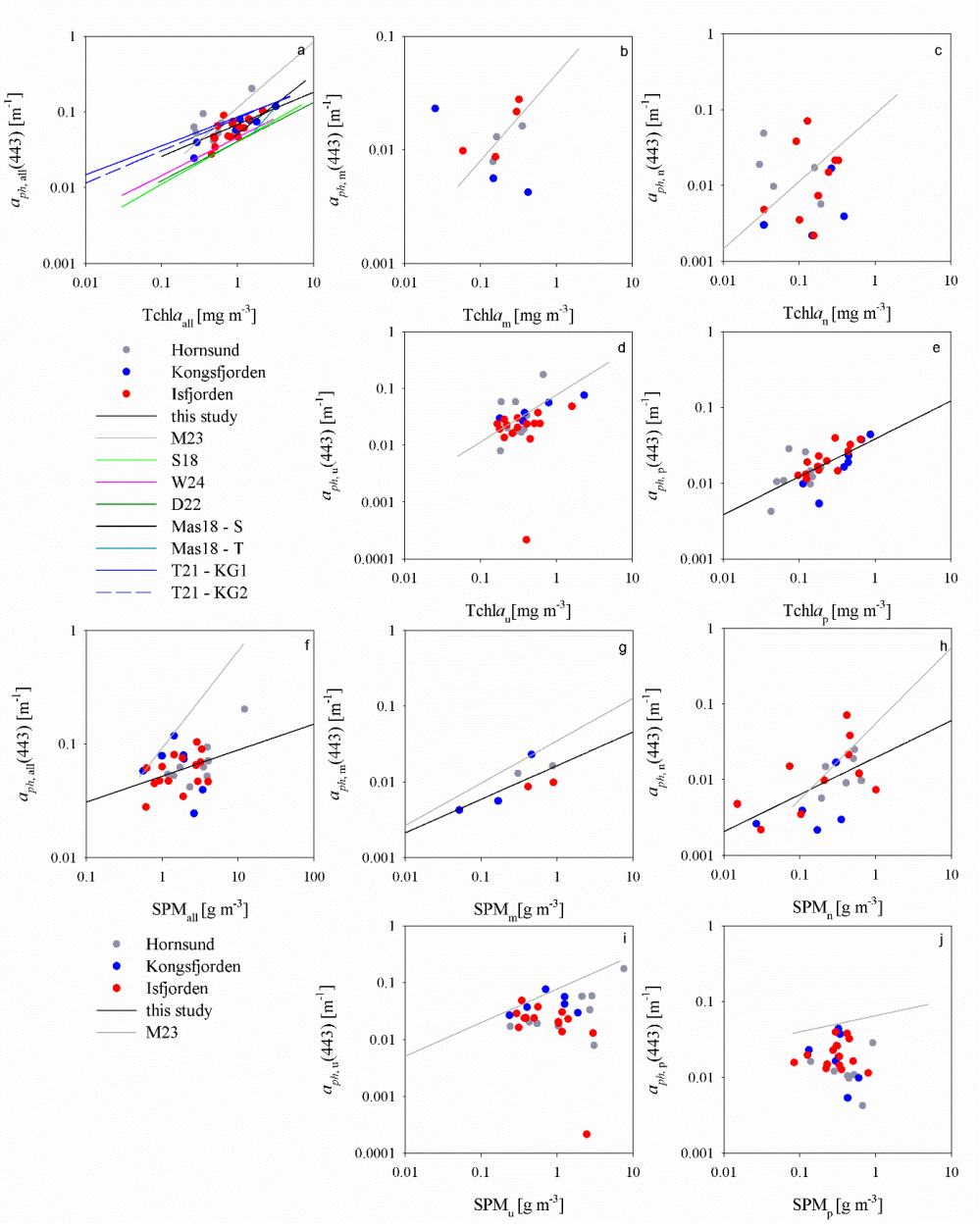

Figure 10: Relationships between absorption coefficients at 443 nm and Tchl*a* (a-e) or SPM (f-j) by all unfractionated phytoplankton (a, f) and in size classes: micro (b, g), nano (c, h), ultra (d, i) and pico (e, j). The black lines indicates the relationships obtained in this study, M23 the relationship in Meler et al. (2023) for the Baltic Sea; S18 show the relationship for Kongsfjorden and Krossfjorden in Son and Kim (2018); W24 show the relationship for fiords and coastal waters of Spitsbergen (Woźniak et al., 2024a); D22 – for Scotian Shelf, Northwest Atlantic Basin, Labrador Sea in Devred et al. (2022); Mas18-S and Mas18-T show the relationships for Norwegian fjords: S - Sognefjord, T – Trondheimsfjord, of Mascarenhas et al. (2018); T21 – Kongsjorden in Tripathy et al. (2021).

https://doi.org/10.5194/egusphere-2025-2800
Preprint. Discussion started: 28 August 2025

Figure 11 shows the relationships of absorption coefficients by CDOM vs the total concentrations of Tchl*a* and SPM. Both relations show a very small correlation, the R^2 values in both cases does not exceed 0.1. For comparison, the figure shows the approximation obtained by Son and Kim (2018) for Kongsfjorden and Krossfjorden. It is clear that it does not reflect the nature of the variability observed in our dataset. In Kongsfjorden, the main source of CDOM is the Atlantic Water from the WSC (Granskog et al., 2012; Pavlov et al., 2015), along with local production related to bacterial activity and degradation of macroalgae that release CDOM substances. The contribution of terrestrial CDOM is relatively minor (Pavlov et al., 2019), which could indicate that the dependence of CDOM vs Tchl*a* may be more accurate in this region. It can be seen that the data from Kongsfjorden and Isfjorden correlate better with Tchl*a* than the CDOM data from Hornsund. This may be due to the differences in quantity or nature of dissolved organic substances flow into Horsund.

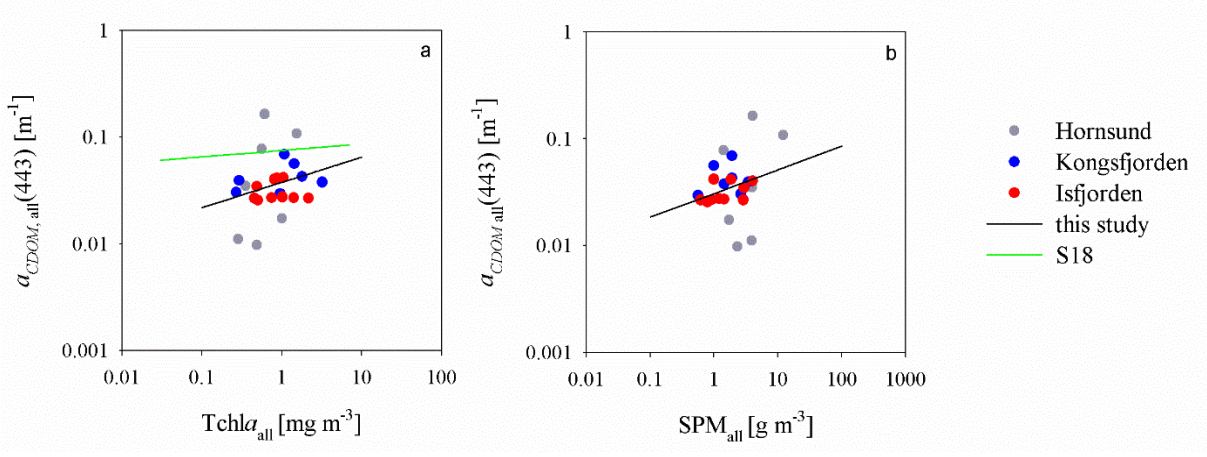

Figure 11: Relationships between CDOM absorption coefficients at 443 mn and Tchl*a* (a) or SPM (b). The black lines indicates the relationships obtained in this study, S18 show the relationship for Kongsfjorden and Krossfjorden in Son and Kim (2018).

4.4 Average chlorophyll- and mass-specific absorption of particles by size class

The analyses enabled the determination of average chlorophyll- and mass-specific light absorption coefficients for particles, detritus and phytoplankton within defined size classes. These coefficients i.e. light absorption coefficients normalized to Tchl*a* or SPM concentrations, are valuable for describing. the relationships between biogeochemical and optical quantities in a simplified yet informative way.

Due to the dominance of ultra-particles in our dataset (accounting for over 70% of the total Tchl*a* and SPM), it was not possible to apply the same procedure for determining the average specific absorption coefficients for the remaining size classes as in Meler et al. (2023). Instead, for each particle size class, we determined only the 'normal' (for all spectra in a given size class, not only for the dominant ones in a given size class) average chlorophyll-specific absorption coefficients $a_p^{(\mathrm{Tchl}a)}(\lambda)$, $a_d^{(\mathrm{Tchl}a)}(\lambda)$

https://doi.org/10.5194/egusphere-2025-2800
Preprint. Discussion started: 28 August 2025

and $a_{ph}^{(Tchl\mathit{a})}(\lambda)$ and the mass average mass-specific absorption coefficients $a_p^{(SPM)}(\lambda)$, $a_d^{(SPM)}(\lambda)$ and $a_{ph}^{(SPM)}(\lambda)$ with standard deviations (Figure 12, left and right panels, respectively). Due to the dominance of inorganic matter (57%) and relatively weak correlations between absorption coefficients by particles (including detritus and phytoplankton) and Tchl*a*, the mean chlorophyll-specific absorption coefficients are characterized by large standard deviations. The mean coefficients $a_p^{(SPM)}(\lambda)$, $a_d^{(SPM)}(\lambda)$ for the analyzed data set are characterized by higher values than for the data set reported by Woźniak et al. (2024b). The standard deviations are also higher, which indicates that in the analyzed data set it was possible to find a wider cross-section of waters with different biogeochemical and absorption properties. The average $a_p^{(SPM)}(\lambda)$ values across size classes are similar, making it difficult to clearly distinguish between them of the average $a_d^{(SPM)}(\lambda)$ and $a_{ph}^{(SPM)}(\lambda)$ show more pronounced inter-class differences. In particular, pico- and ultra-particles are characterized by lower values in the 350-400 nm spectral range with a clearly marked maximum at 443 nm, while micro- and nano-particles do not have such a clear maximum at 443 nm.

According to Ciotti et al. (2002) the spectral averages of $a_{ph}^{(Tchl\mathit{a})}(\lambda)$ should have the lowest values for the micro-particles class and the highest for the pico-particles class. In our study, the lowest values were observed for pico- and ultra-particles, higher for micro-particles and the highest for nano-particles.

Table 5 summarizes the average values of $a_p^{(Tchl\mathit{a})}(\lambda)$, $a_d^{(Tchl\mathit{a})}(\lambda)$, $a_{ph}^{(Tchl\mathit{a})}(\lambda)$ and $a_p^{(SPM)}(\lambda)$, $a_d^{(SPM)}(\lambda)$, $a_{ph}^{(SPM)}(\lambda)$ for different particle size classes, together with their standard deviations, at selected wavelengths corresponding to the OLCI sensor bands (400 nm, 443 nm, 510 nm, 620 nm, 675 nm and 709 nm). Comparing the obtained average values with those presented in Meler et al. (2023) for the Baltic Sea, the results reveal significant differences in absorption and biogeochemical properties between Arctic fjords and Baltic coastal waters. Mean values of $a_p^{(Tchl\mathit{a})}(\lambda)$, $a_d^{(Tchl\mathit{a})}(\lambda)$ and $a_{ph}^{(Tchl\mathit{a})}(\lambda)$ for the analyzed data set are several times higher than those obtained for the Baltic Sea, depending on the particle size class. This may be partly due to the difference in the method of determining the mean values of the light absorption coefficients. In the case of the Baltic Sea data, the mean coefficients were determined for samples dominated by specific size class. In the fjord samples, due to the dominance of ultra-particles, the average absorption coefficients were calculated from all samples for each size class. However, the greatest influence on such a large discrepancy between the average values of the coefficients $a_p^{(Tchl\mathit{a})}(\lambda)$, $a_d^{(Tchl\mathit{a})}(\lambda)$ and $a_{ph}^{(Tchl\mathit{a})}(\lambda)$ in these two different water bodies is the difference in the nature of the relationship between particles and Tchl*a* concentrations. In the Baltic Sea, the coefficients $a_p(\lambda)$, $a_d(\lambda)$ and $a_{ph}(\lambda)$ were better correlated with Tchl*a* concentrations, so also the coefficients normalized to Tchl*a* showed a better relationships. In the fjords, however, the relationships of the coefficients $a_p(\lambda)$, $a_d(\lambda)$ and $a_{ph}(\lambda)$ correlated weakly with Tchl*a*, which is also reflected in the case of normalized light absorption coefficients. In the case of average values of $a_p^{(SPM)}(\lambda)$, $a_d^{(SPM)}(\lambda)$ and $a_{ph}^{(SPM)}(\lambda)$, the differences are not so significant, but it can also be seen that in most cases they are slightly higher than those for the Baltic Sea.

https://doi.org/10.5194/egusphere-2025-2800
Preprint. Discussion started: 28 August 2025

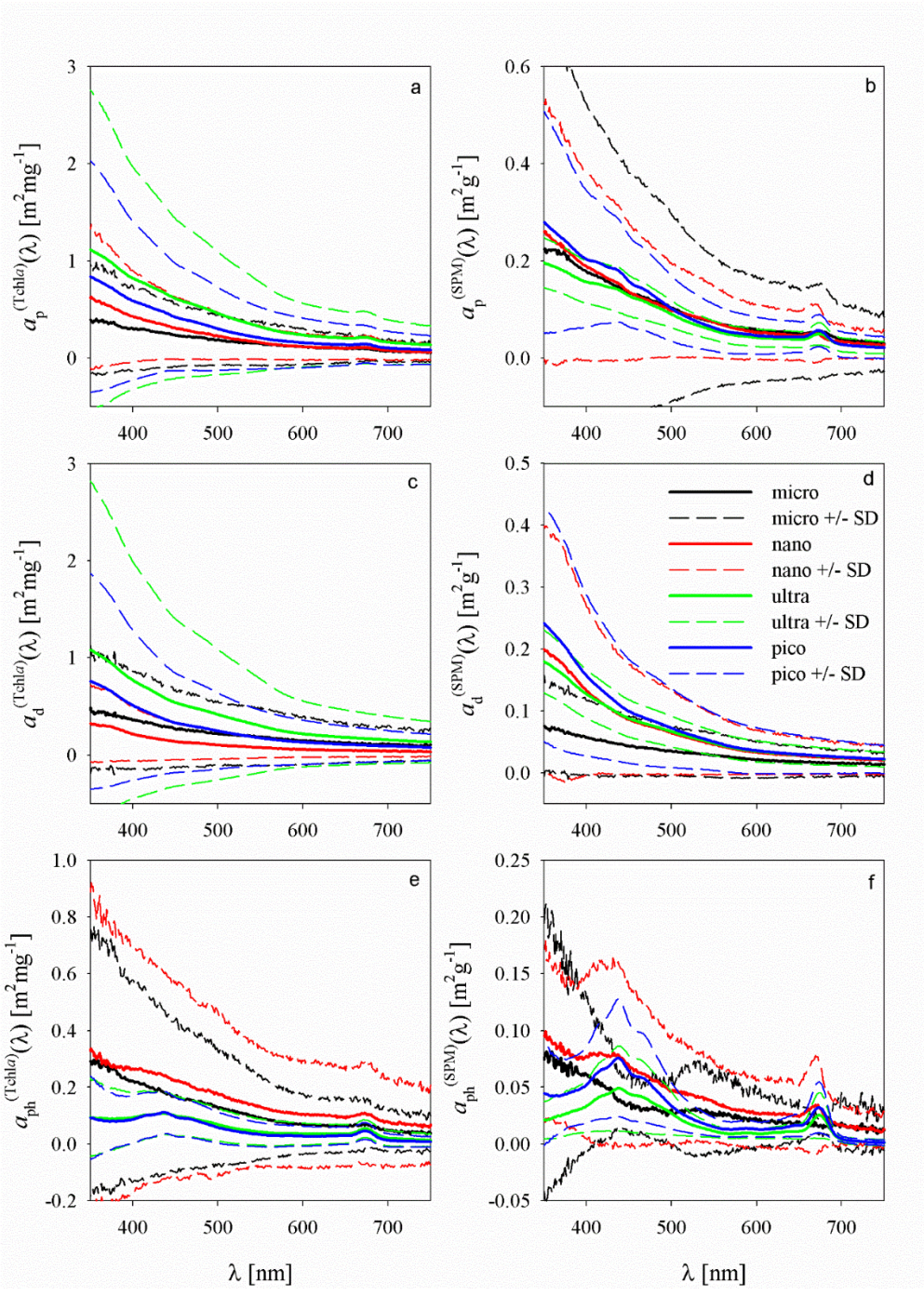

Figure 12: Average chlorophyll-specific (left panel) and mass-specific (right panel) light absorption coefficients ± SD for all particles (a, b), detritus (c, d) and phytoplankton (e, f) for size classes : micro-, nano-, ultra- and picoplankton.

https://doi.org/10.5194/egusphere-2025-2800
Preprint. Discussion started: 28 August 2025

Table 5: Average values of chlorophyll-specific and mass-specific light absorption coefficients ± SD for all particles, detritus and phytoplankton calculated for size classes : micro-, nano-, ultra- and picoplankton at selected wavelengths corresponding to selected bands of the OLCI sensor.

	400 nm	443 nm	510 nm	620 nm	675 nm	709 nm
$a_{p,micro}^{(Chl a)}(\lambda)$	0.308+/-0.440	0.253+/-0.348	0.170+/-0.233	0.108+/-0.164	0.095+/-0.120	0.073+/-0.113
$a_{p,nano}^{(Chl a)}(\lambda)$	0.429+/-0.471	0.325+/-0.334	0.211+/-0.224	0.111+/-0.127	0.108+/-0.116	0.076+/-0.093
$a_{p,ultra}^{(Chl a)}(\lambda)$	0.823+/-1.146	0.645+/-0.861	0.430+/-0.595	0.222+/-0.304	0.213+/-0.265	0.154+/-0.219
$a_{p,pico}^{(Chl a)}(\lambda)$	0.591+/-0.818	0.451+/-0.581	0.279+/-0.401	0.147+/-0.236	0.143+/-0.192	0.097+/-0.166
$a_{d,micro}^{(Chl a)}(\lambda)$	0.361+/-0.501	0.285+/-0.414	0.212+/-0.315	0.137+/-0.228	0.110+/-0.187	0.106+/-0.172
$a_{d,nano}^{(Chl a)}(\lambda)$	0.215+/-0274	0.149+/-0.200	0.096+/-0.135	0.053+/-0.075	0.046+/-0.063	0.042+/-0.059
$a_{d,ultra}^{(Chl a)}(\lambda)$	0.772+/-1.220	0.566+/-0.901	0.393+/-0.631	0.201+/-0.313	0.168+/-0.261	0.151+/-0.237
$a_{d,pico}^{(Chl a)}(\lambda)$	0.513+/-0.773	0.351+/-0.539	0.232+/-0.367	0.122+/-0.211	0.101+/-0.174	0093+/-0.161
$a_{ph,micro}^{(Chl a)}(\lambda)$	0.222+/-0.357	0.178+/-0.281	0.123+/-0.193	0.066+/-0.098	0.069+/-0.090	0.046+/-0.077
$a_{ph,nano}^{(Chl a)}(\lambda)$	0.266+/-0.432	0.232+/-0.352	0.165+/-0.264	0.101+/-0.178	0.103+/-0.171	0.071+/-0.143
$a_{ph,ultra}^{(Chl a)}(\lambda)$	0.093+/-0.091	0.105+/-0.072	0.060+/-0.055	0.035+/-0.037	0.053+/-0.031	0.019+/-0.026
$a_{ph,pico}^{(Chl a)}(\lambda)$	0.086+/-0.083	0.106+/-0.071	0.051+/-0.052	0.027+/-0.033	0.045+/-0.029	0.011+/-0.023
$a_{p,micro}^{(SPM)}(\lambda)$	0.179+/-0.345	0.143+/-0.265	0.096+/-0.18	0.056+/-0.101	0.056+/-0.099	0.038+/-0.071
$a_{p,nano}^{(SPM)}(\lambda)$	0.189+/-0.193	0.146+/-0.153	0.093+/-0.092	0.051+/-0.055	0.047+/-0.055	0.033+/-0.033
$a_{p,ultra}^{(SPM)}(\lambda)$	0.157+/-0.044	0.136+/-0.045	0.082+/-0.025	0.040+/-0.018	0.050+/-0.023	0.025+/-0.014
$a_{p,pico}^{(SPM)}(\lambda)$	0.204+/-0.141	0.172+/-0.101	0.092+/-0.063	0.044+/-0.035	0.056+/-0.033	0.025+/-0.025
$a_{d,micro}^{(SPM)}(\lambda)$	0.057+/-0.060	0.045+/-0.050	0.033+/-0.038	0.020+/-0.028	0.016+/-0.023	0.015+/-0.021
$a_{d,nano}^{(SPM)}(\lambda)$	0.139+/-0.136	0.095+/-0.093	0.063+/-0.064	0.032+/-0.033	0.016+/-0.028	0.024+/-0.026
$a_{d,ultra}^{(SPM)}(\lambda)$	0.127+/-0.039	0.092+/-0.031	0.062+/-0.024	0.032+/-0.016	0.027+/-0.014	0.024+/-0.013
$a_{d,pico}^{(SPM)}(\lambda)$	0.157+/-0.131	0.105+/-0.089	0.067+/-0.060	0.033+/-0.034	0.027+/-0.029	0.025+/-0.026
$a_{ph,micro}^{(SPM)}(\lambda)$	0.061+/-0.06	0.037+/-0.024	0.029+/-0.035	0.020+/-0.022	0.017+/-0.007	0.014+/-0.019
$a_{ph,nano}^{(SPM)}(\lambda)$	0.078+/-0.073	0.035+/-0.077	0.046+/-0.045	0.028+/-0.032	0.031+/-0.038	0.015+/-0.015
$a_{ph,ultra}^{(SPM)}(\lambda)$	0.034+/-0.023	0.048+/-0.036	0.022+/-0.015	0.026+/-0.005	0.025+/-0.020	0.003+/-0.003
$a_{ph,pico}^{(SPM)}(\lambda)$	0.052+/-0.033	0.072+/-0.049	0.028+/-0.016	0.013+/-0.007	0.032+/-0.022	0.003+/-0.002

https://doi.org/10.5194/egusphere-2025-2800
Preprint. Discussion started: 28 August 2025

5 Conclusions

The conducted studies provides important information on the role of particle size and its contribution to the total concentrations of SPM, Tchl*a* and absorption properties of suspended matter in the waters of three selected fjords of Spitsbergen. Currently, there are many efforts aimed at extracting as much information as possible from the color of water using remote sensing methods. These go beyond estimating the concentration of chlorophyll *a*, but also aim to retrieve other biological parameters, such as the size structure of phytoplankton population and light absorption by individual water components, which can serve as proxies for estimating organic carbon pool in the ocean. Various models are created, to recover physical, biological and chemical data from satellite observations. However, such approaches require empirical studies, which indicate regional differences between water bodies. Empirical fractionation, as conducted in this study, provides general information on the size structure and composition of suspended particles in fjord waters.

Our results show that particles of different sizes can exhibit large variability in absorption properties, and similar ranges of variability can occur across particle size classes. This may complicate unambiguous identification of the particle size class based solely on the light absorption spectrum. Due to the limited number of samples and the high heterogeneity of optically active substances in fjord waters, the presented analyses should be treated as qualitative results, similarly to Meler et al. (2023). Further, multi-seasonal and comprehensive studies are necessary to fully understand the dynamics of suspended particles. Limitations of the cascade filtration method, such as imperfect size separation of particles (due to irregular particle shapes – not always spherical), problems with mesh filters, rapid sedimentation of large particles), may lead to partial over- or underestimation of results, as mentioned by Koestner et al. (2019) and Meler et al. (2023).

Our results and those presented by other authors (e.g. Son and Kim, 2018; Halbach et al., 2019; Woźniak et al., 2024) show that the bio-optical characteristics of western Svalbard fjords vary greatly during summer. This is due to the very complex environmental characteristics of the fjords (tidal glaciers, atmospheric and hydrological conditions, etc.). Our study focuses on the summer season, when there is a high phytoplankton productivity (Assmy et al., 2023; Chitkara et al., 2024). Based on our analyses, it is possible to observe the variability of particle size distributions not only for the entire fjord data set, but also in individual fjords. Ultra-particles (2-5 µm) dominated suspended particles (average SPM_{ultra}/SPM=51%) and were mainly inorganic (average PIM/SPM=67%). The fjord-specific values were: Hornsund, SPM_{ultra}/SPM = 53%,PIM/SPM=76%, Kongsfjorden, SPM_{ultra}/SPM = 53% and PIM/SPM=63%, and Isfjorden, SPM_{ultra}/SPM=48% and PIM/SPM=64%.

We observed that the largest contribution to particle absorption was from detritus, defined as organic and inorganic detritus plus mineral particles. For the selected wavelength of 443 nm, the contribution of detritus to particle absorption, $a_d(443)/a_p(443)$, was on average 66%, and varied by fjord: 76% in Hornsund, 60% in Kongsjorden and 63% in Isfjorden. We also observed that ultra-particles often had a dominant contribution to $a_p(443)$, $a_d(443)$ (approx. 60% and higher) and $a_{ph}(443)$ (approx. 45% and higher). Pico-particles contributed from 20% to 32% of the light absorption, followed by nano-particles from 6% to 26% and the smallest contribution was given by micro-particles from 1% to 12.6%.

https://doi.org/10.5194/egusphere-2025-2800
Preprint. Discussion started: 28 August 2025

Analysis of the variability of light absorption coefficients by different size fractions of particles suspended in sea water in fjords in relation to the characteristics describing this suspended matter (i.e., Tchl*a* and SPM) showed generally weak correlations for Tchl*a* and slightly stronger for SPM. It is possible that expending the dataset would allow obtaining better correlations, which indicates the need to continued research in this area. A better understanding of the influence of particle size on the absorption properties of Arctic fjord waters can support methods for remote estimation of phytoplankton sizes in this area. Measurements of chlorophyll- and mass-specific light absorption coefficients of suspended particles, including detritus and phytoplankton, are essential to develop optical inversions algorithms for mapping the biogeochemical components present in surface waters and to better understand the origin of optical signatures in remote sensing studies. To date, most literature has reported a_p, a_d, a_{ph} coefficients as functions of Tchl*a* or SPM for the total suspended matter, without taking into account the particle size. Recent studies (Meler et al., 2023 or Woźniak et al., 2024b) have begun to explore these relationships across size classes of particles obtained by fractionation However, the relationships presented by other authors were obtained indirectly, based on, for example, diagnostic pigment analysis (DPA) and size structure (Vidussi et al., 2001; Uitz et al., 2008) or on the basis of HPLC data and the pigment size-class model (Brewin et al. 2010). Although there are many methods for determining phytoplankton size in marine environments (IOCCG report, 2014),direct studies of different particle size classes are essential in order to determine direct relationships between different characteristics of marine ecosystems.

Data availability:

The in situ absorption data (absorption by particles, detritus, phytoplankton and CDOM) and biogeochemical data (concentration of Tchl*a* and SPM) can be acquired for scientific research purposes upon request from Justyna Meler

Authors contribution:

Conceptualization, J.M.; methodology, J.M., J.S-E, M.Z.; validation, J.M, J.S-E, M.Z.; formall analysis, J.M.; investigation, J.M.; resources, J.M, J.S-E, M.Z., data curation, J.M., M.Z,; writing—original draft preparation, J.M.; writing—review and editing, M.Z., J.S-E; visualization, J.M.; supervision, M.Z., J.S-E. All authors have read and agreed to the published version of the manuscript.

Conflicts of Interest:

The authors declare that they have no conflict of interest.

Acknowledgments:

This research was carried out as part of the project DOMinEA funded by the National Science Centre, Poland, entitled ‘Impact of hydrological regimes on the quantitative and qualitative optical properties of dissolved organic matter in West Spitsbergen fiords’ (contract No. 2021/41/B/ST10/03603) (awarded to Monika Zabłocka) and as part of Statutory Research Project (No.I.1) of the Institute of Oceanology Polish Academy of Sciences in Sopot. We are grateful to Dagmara Litwicka for help in collecting the empirical material.

https://doi.org/10.5194/egusphere-2025-2800
Preprint. Discussion started: 28 August 2025

References

Assmy, P., Kvernvik, A. C., Hop, H., Hoppe, C. J.M., Chierici, M., Divya, D. T., Duarte, P., Fransson, A., García, L. M., Patuła, W., Kwaśniewski, S., Maturilli, M., Pavlova, O., Tatarek, A., Wiktor, J. M., Wold, A., Wolf, K.K.E., and Bailey, A.: Seasonal plankton dynamics in Kongsfjorden during two years of contrasting environmental conditions, Progr. Oceanogr., 213, https://doi.org/10.1016/j.pocean.2023.102996, 2023.

Balch, W.M., Drapeau, D.T., Bowler, B.C., Lyczskowski, E., Booth, E.S., and Alley, D.: The Contribution of Coccolithophores to the Optical and Inorganic Carbon Budgets during the Southern Ocean Gas Exchange Experiment: New Evidence in Support of the "Great Calcite Belt" Hypothesis. J. Geophys. Res. Oceans, 116, C00F06, https://doi.org/10.1029/2011JC006941, 2011.

Beszczynska-Moller, A., Fahrbach, E., Schauer, U., and Hansen, E.: Variability in Atlantic water temperature and transport at the entrance to the Arctic Ocean, 1997–2010. ICES J. Mar. Sci. 69, 852–863, 2012.

Bianchi, T. S., Arndt, S., Austin, W. E. N., Benn, D. I., Bertrand, S., Cui, X., Faust, J. C., Koziorowska-Makuch, K., Moy, C. M., Savage, C., Smeaton, C., Smith, R. W., and Syvitski, J.: Fjords as Aquatic Critical Zones (ACZs), Earth-Sci. Rev., 203, 103145, https://doi.org/10.1016/j.earscirev.2020.103145, 2020,

Błaszczyk, M., Jania, J.A., and Kolondra, L.: Fluctuations of tide-water glaciers in Hornsund Fjord (Southern Svalbard) since the beginning of the 20th century. Pol. Polar Res. 34 (4), 327—352, http://dx.doi.org/10.2478/popore-2013-0024, 2013.

Błaszczyk, M., Ignatiuk, D., Uszczyk, A., Cielecka-Nowak, K., Gtrabiec, M., Jania, J.A., Moskalik, M. and Walczowski, W.: Freshwater input to the Arctic fjord Hornsund (Svalbard), Polar Res, 38, https://doi.org/10.33265/polar.v38.3506, 2019.

Braeckman, U., Pasotti, F., Hoffmann, R., Vázquez, S., Wulff, A., Schloss, I.R., Falk, U., Deregibus, D., Lefaible, N., Torstensson, A., Al-handal, A., Wenzhöfer, F., and Vanreusel, A.: Glacial melt disturbance shifts community metabolism of an Antarctic seafloor ecosystem from net autotrophy to heterotrophy. Commun. Biol. 4, 1—11. https://doi.org/10.1038/s42003-021-01673-6, 2021.

Brewin, R.J.W., Sathyendranath, S., Hirata, T., Lavender, S.J., Barciela, R.M., and Hardman-Mountford, N.J.: A three-component model of phytoplankton size class for the Atlantic Ocean, Ecol. Model. 221, 1472–1483, https://doi.org/10.1016/j.ecolmodel.2010.02.014, 2010.

Calleja, M.L., Kerhervé, P., Bourgeois, S., Kędra, M., Leynaert, A., Devred, E., Babin, M., and Morata, N.: Effects of increase glacier discharge on phytoplankton bloom dynamics and pelagic geochemistry in a high Arctic fjord. Progr. Oceanogr., 159, 195–210, https://doi. org/10.1016/j.pocean.2017.07.005, 2017.

Chitkara, C., Juul-Pedersen, T., Krawczyk, D., Søreide, J.E., Vader, A., Gradinger, R., Winding, M.H.S., and Vonnahme, T.R.: Seasonality in phytoplankton communities and production in three Arctic fjords across a climate gradient, Prog. Oceanogr. 227, https://doi.org/10.1016/j.pocean.2024.103317, 2024

Ciotti, A.M., Lewis, M.R., and Cullen, J.J.: Assessment of the relationships between dominant cell size in natural phytoplankton communities and the spectral shape of the absorption coefficient, Limnol. Oceanogr., 47, 404–417, https://doi.org/10.4319/lo.2002.47.2.0404, 2002.

https://doi.org/10.5194/egusphere-2025-2800
Preprint. Discussion started: 28 August 2025

Clark, G.F., Stark, J.S., Palmer, A.S., Riddle, M.J., and Johnston, E.L.: The roles of sea-ice, light and sedimentation in structuring shallow antarctic benthic communities. PLoS One 12, 1-20. https://doi.org/10.1371/journal.pone.0168391, 2017.

Cottier, F., Tverberg, V., Inall, M., et al.: Water mass modification in an Arctic fjord through cross-shelf exchange: the seasonal hydrography of Kongsfjorden. Svalbard. J. Geophys. Res. 110, C12005. https://doi.org/10.11029/12004JC002757, 2005.

Cottier, F.R., Nilsen, F., Inall, M.E., Gerland, S., Tverberg, V., and Svendsen, H.: Wintertime warming of an Arctic shelf in response to large-scale atmospheric circulation. Geophys. Res. Lett. 34. https://doi.org/10.1029/2007gl029948, 2007.

Cottier, F.R., Nilsen, F., Skogseth, R., Tverberg, V., Skarðhamar, J., and Svendsen, H.: Arctic fjords: A review of the oceanographic environment and dominant physical processes. *Geological Society of London*, *344*, 35–50. https:// doi. org/ 10. 1144/ SP344.4, 2010.

Darlington, E.: Meltwater Delivery from the Tidewater Glacier Kronebreen to Kongsfjorden, Svalbard; Insights from in situ and Remote-Sensing Analyses of sediment plumes (PhD Thesis). Loughborough University, 2015.

Davies, E. J., McKee, D., Bowers, D., Graham, G. W., and Nimmo-Smith, W. A. M.: Optically significant particle sizes in seawater, Appl. Optics, 53, 1067–1074, https://doi.org/10.1364/AO.53.001067, 2014.

Decembrini, F., Bergamasco, A., and Mangoni, O.: Seasonal characteristics of size-fractionated phytoplankton community and fate of photosynthesized carbon in a sub-Antarctic area (Straits of Magellan), J. Mar. Sys., 136, 31–41, https://doi.org/10.1016/j.jmarsys.2014.03.008, 2014.

Deja, K., Ormańczyk, M., and Dragańska-Deja, K.: Plankton or benthos: where krill belongs in Spitsbergen fjords? (Svalbard Archipelago, Arctic). Polar Biol 42, 1415-1430. https://doi.org/ 10.1007/s00300-019-02524-1, 2019.

Deja, K., Węsławski, J.M., Borszcz, T., Włodarska-Kowalczuk, M., Kukliński, P., Bałazy, P., and Kwiatkowska, P.: Recent distribution of Echinodermata species in Spitsbergen coastal wa- ters. Pol. Polar Res. 37, 511-526. https://doi.org/10.1515/ popore-2016-0027, 2016.

Devred, E., Perry, T., and Massicotte, P.: Seasonal and decadal variations in absorption properties of phytoplankton and non-algal particulate matter in three oceanic regimes of the Northwest Atlantic. Front. Mar. Sci. 9:932184. doi: 10.3389/fmars.2022.932184, 2022,

Dragańska-Deja, K.: Characterization of suspended particles at different glacial bays at Spitsbergen, Oceanologia, 66, 2, https://doi.org/10.1016/j.oceano.2023.12.001, 2024.

D'Sa, E. J. and Ko, D. S.: Short-term influences on suspended particulate matter distribution in the Northern Gulf of Mexico: Satellite and model observations, Sensors, 8, 4249–4264, https://doi.org/10.3390/s8074249, 2008.

D'Sa, E. J., Miller, R. L., and Del Castillo, C.: Bio-optical properties and ocean color algorithms for coastal waters influenced by the Mississippi River during a cold front, Appl. Optics, 45, 7410–7428, https://doi.org/10.1364/AO.45.007410, 2006.

Dunse, T., Dong, K., Aas, K.S. and Stige, L.C.: Regional-scale phytoplankton dynamics and their association with glacier meltwater runoff in Svalbard, Biogeosciences, 19, 2, 271-294, https://doi.org/10.5194/bg-19-271-2022, 2022,

https://doi.org/10.5194/egusphere-2025-2800
Preprint. Discussion started: 28 August 2025

Eleveld, M.A., van der Wal, D., and van Kessel, T.: Estuarine suspended particulate matter concentrations from sun synchronous satellite remote sensing: Tidal and meteorological effects and biases, Remote Sens. Environ., 143, 2014–215, https://doi.org/10.1016/j.rse.2013.12.019, 2014.

Finne, E.A., Varpe, Ø., Durant, J.M., Gabrielsen, G.W., and Poste, A.E.: Nutrient fluxes from an Arctic seabird colony to the adjacent coastal marine ecosystem, Polar Biol., https://doi.org/10.1007/s00300-022-03024-5, 2022.

Gao, K., Beardall, J., Häder, D.P., Hall-Spencer, J.M., Gao, G., and Hutchins, D.A.: Effects of ocean acidification on marine photosynthetic organisms under the concurrent influences of warming, UV radiation, and deoxygenation. Front. Mar. Sci., 6, 1–18. https://doi.org/10.3389/fmars.2019.00322, 2019.

Granskog, M. A., Stedmon, C. A.,. Dodd, P. A, Amon, R. M. W.,. Pavlov, A. K, de Steur, L., and Hansen, E.: Characteristics of colored dissolved organic matter (CDOM) in the Arctic outflow in the Fram Strait: Assessing the changes and fate of terrigenous CDOM in the Arctic Ocean, J. Geophys. Res., 117, C12021, doi:10.1029/2012JC008075, 2012.

Granskog ,M.A., Pavlov, A.K., Sagan, S., Kowalczuk, P., Raczkowska, A., and Stedmon, C.A.: Effect of sea-ice melt on inherent optical properties and vertical distribution of solar radiant heating in Arctic surface waters. J. Geophys. Res: Oceans. doi:10.1002/2015JC011087, 2015.

Guidi, L., Stemmann, L., Jackson, G.A. , Ibanez, F., Claustre, H., Legendre, L., Picheral, M., and Gorskya, G.: Effects of phytoplankton community on production, size, and export of large aggregates: A world-ocean analysis, Limnol. Oceanogr., 54, doi: 10.4319/lo.2009.54.6.1951, 2009.

Halbach, L., Vihtakari, M., Duarte, P., Everett, A., Granskog, M.A., Hop, H., Kauko, H.M., Kristiansen, S., Myhre, P.I., Pavlov, A.K., Pramanik, A., Tatarek, A., Torsvik, T., Wiktor, J.M., Wold, A., Wulff, A., Steen, H., and Assmy, P.: Tidewater Glaciers and Bedrock Characteristics Control the Phytoplankton Growth Environment in a Fjord in the. Arctic. Front. Mar. Sci. 6. https:// doi.org/10.3389/fmars.2019.00254, 2019.

Hegseth, E.N., Assmy, P., Wiktor, J., Wiktor, J.M., Kristiansen, S., Leu, E., Tverberg, V., Gabrielsen, T.M., Skoseth, R. and Cottier, F.: Phytoplankton seasonal dynamics in Kongsfjorden, Svalbard and the adjacent shelf. In: Hop, H., Wiencke, C. (Eds.), The ecosystem of Kongsfjorden, Svalbard. Advances in Polar Ecology 2, Springer, Cham. pp. 173–227. http://dx.doi.org/10.1007/978-3-319-46425-1_6, 2019.

Hirata, T., Aiken, J., Hardman-Mountford, N.J., Smyth, T.J., and Barlow, R.G.: An absorption model to determine phytoplankton size classes from satellite ocean colour, Remote Sens. Environ., 112, 3153–3159, https://doi.org/10.1016/j.rse.2008.03.011, 2008.

Holinde, L., and Zielinski, O.: Bio-optical characterization and light availability parameterization in Uummannaq Fjord and Vaigat–Disko Bay (West Greenland). Ocean Science 12(1), 117-128, 2016.

IOCCG: Phytoplankton functional types from space, Reports of the International Ocean-Colour Coordinating Group, edited by: Sathyendranath, S., No. 15, IOCCG, Dartmouth, Canada, 154 pp., https://doi.org/10.25607/OBP-106, 2014.

https://doi.org/10.5194/egusphere-2025-2800
Preprint. Discussion started: 28 August 2025

Koestner, D., Stramski, D., and Reynolds, R.: Assessing the effects of particle size and composition on light scattering through measurements of size-fractionated seawater samples, Limnol. Oceanogr., 65, 173–190, https://doi.org/10.1002/lno.11259, 2019.

Konik, M., Darecki, M., Pavlov, A. K., Sagan, S., and Kowalczuk, P.: Darkening of the Svalbard Fjords Water Observed With Satellite Ocean olor Imagery in 1997-2019. Front. Mar. Sci. 8, 699318. https://doi.org/10.3389/fmars.2021.699318, 2021.

Lam, P. J., Ohnemus, D. C., and Auro, M. E.: Size-fractionated major particle composition and concentrations from the US GEOTRACES North Atlantic Zonal Transect, Deep-Sea Res. Pt. II, 116, 303–320, https://doi.org/10.1016/j.dsr2.2014.11.020, 2015.

Lam, P. J., Lee, J.-M., Heller, M. I., Mehic, S., Xiang, Y., and Bates, N. R.: Size-fractionated distributions of suspended particle concentration and major phase composition from the U.S. GEOTRACES Eastern Pacific Zonal Transect (GP16), Mar. Chem., 201, 90–107, https://doi.org/10.1016/j.marchem.2017.08.013, 2018.

Le Quéré, C., Harrison, S. P., Prentice, C. I., Buitenhuis, E. T., Aumont, O., Bopp, L., Claustre, H., Cotrim da Cunha, L., Geider, R., Giraud, X., Klass, C., Kohfeld, K. E., Legendre, L., Manizza, M., Platt, T., Rivkin, R., Sathyendranath, R. B., Uitz, J., Watson, A. J., and Wolf-Gladrow, D.: Ecosystem dynamics based on plankton functional types for global ocean biogeochemistry models, Glob. Change Biol., 11, 2016–2040, https://doi.org/10.1111/j.1365-2486.2005.1004.x, 2005.

Lund-Hansen, L. C., Andersen, T. J., Nielsen, M. H., and Pejrup, M.: Suspended Matter, Chl-a, CDOM, Grain Sizes, and Optical Properties in the Arctic Fjord-Type Estuary, Kangerlussuaq, West Greenland During Summer, Estuar. Coast., 33, 1442–1451, https://doi.org/10.1007/S12237-010-9300-7/FIGURES/5, 2010.

Marañón, E., Holligan, P. M., Barciela, R., González, N., Mouriño, B., Pazó, M. J., and Varela, M.: Patterns of phytoplankton size structure and productivity in contrasting open-ocean environments, Mar. Ecol. Prog. Ser., 216, 43–56, https://www.jstor.org/stable/24864737 (last access: 28 June 2023), 2001.

Mascarenhas, V. J. and Zielinski, O.: Parameterization of Spectral Particulate and Phytoplankton Absorption Coefficients in Sognefjord and Trondheimsfjord, Two Contrasting Norwegian Fjord Ecosystems, Remote Sens., 10(6):977. https://doi.org/10.3390/rs10060977, 2018.

Mascarenhas, V. J. and Zielinski, O.: Hydrography-Driven Optical Domains in the Vaigat-Disko Bay and Godthabsfjord: Effects of Glacial Meltwater Discharge, Front. Mar. Sci., 6, 335, https://doi.org/10.3389/fmars.2019.00335, 2019.

Mascarenhas, V., Voß, D., Wollschlaeger, J., and Zielinski, O.: Fjord light regime: Biooptical variability, absorption budget, and hyperspectral light availability in Sognefjord and Trondheimsfjord, Norway. J. Geophys. Res.:Oceans, 122(5), 3828-3847, 2017.

Matsuoka, A., Hill, V., Huot, Y., Babin, M., and Bricaud, A.: Seasonal variability in the light absorption properties of western Arctic waters: parameterization of the individual components of absorption for ocean color applications. J. Geophys. Res. 116, C02007. https://doi.org/10.1029/2009JC005594, 2011.

https://doi.org/10.5194/egusphere-2025-2800
Preprint. Discussion started: 28 August 2025

McGovern, M., Pavlov, A.K., Deininger, A., Granskog, M.A., Leu, E., Søreide, J.E., and Poste, A.E.: Terrestrial Inputs Drive Seasonality in Organic Matter and Nutrient Biogeochemistry in a High Arctic Fjord System (Isfjorden, Svalbard), Front. Mar. Sci., 7, 542563, https://doi.org/10.3389/fmars.2020.542563, 2020.

McKee, D. and Cunningham, A.: Identification and characterization of two optical water types in the Irish Sea from in situ inherent optical properties and seawater constituents, Estuar. Coast. Shelf S., 68, 305–316, https://doi.org/10.1016/j.ecss.2006.02.010, 2006.

Meier, W.N., Hovelsrud, G.K., van Oort, B.E.H., Key, J.R., Kovacs, K.M., Michel, C., Haas, C., Granskog, M.A., Gerland, S., Perovich, D.K., Makshtas, A., and Reist, J.D.: Arctic sea ice in transformation: A review of recent observed changes and impacts on biology and human activity, Rev. Geophys., 52, 185–217, doi:10.1002/2013RG000431, 2014.

Meler, J., Litwicka, D., Zabłocka, M.: Variability of light absorption coefficients by different size fractions of suspensions in the southern Baltic Sea, Biogeosciences 20, 2525–2551, https://doi.org/10.5194/bg-20-2525-2023, 2023.

Meler, J., Ostrowska, M., Stoń-Egiert, J., and Zabłocka, M.: Seasonal and spatial variability of light absorption by suspended particles in the southern Baltic: a mathematical description, J. Mar. Sys., 170, 68–87, https://doi.org/10.1016/j.jmarsys.2016.10.011, 2017.

Meler, J.,Woźniak, S. B., and Stoń-Egiert, J.: Comparison of methods for indirectly estimating the phytoplankton population size structure and their preliminary modifications adapted to the specific conditions of the Baltic Sea, J. Mar. Sys, 212, 103446, https://doi.org/10.1016/j.jmarsys.2020.103446, 2020.

Mohammadpour, G., Gagné, J.-P., Larouche, P., and Montes-Hugo, M. A.: Optical properties of size fractions of suspended particulate matter in littoral waters of Québec, Biogeosciences, 14, 5297–5312, https://doi.org/10.5194/bg-14-5297-2017, 2017.

Morel, A. and Bricaud, A.: Theoretical results concerning light absorption in a discrete medium, and application to specific absorption of phytoplankton, Deep-Sea Res., 28, 1375–1393, https://doi.org/10.1016/0198-0149(81)90039-X, 1981.

Nilsen, F., Cottier, F., Skogseth, R., and Mattsson, S.: Fjord-shelf exchanges controlled by ice and brine production: the interannual variation of Atlantic Water in Isfjorden, Svalbard, Cont. Shelf Res. 28, 1838–1853. https://doi.org/10.1016/j.csr.2008.04.015, 2008.

Organelli, E., Bricaud, A., Antoine, D., and Uitz, J.: Multivariate approach for the retrieval of phytoplankton size structure from measured light absorption spectra in the Mediterranean Sea (BOUSSOLE site), Appl. Optics, 52, 2257–2273, https://doi.org/10.1364/AO.52.002257, 2013.

Pavlov, A.K., Tverberg, V., Ivanov, B.V., Nilsen, F., Falk-Petersen, S., and Granskog, M.A.: Warming of Atlantic Water in two Spitsbergen fjords over the last century (1912—2009), Polar Res. 32 (1), 11206, http://dx.doi.org/10.3402/polar.v32i0.11206, 2013.

Pavlov, A.K., Granskog, M.A., Stedmon, C.A., Ivanov, B.V., Hudson, S.R., and Falk-Petersen, S.: Contrasting optical properties of surface waters across the Fram Strait and its potential biological implications, J. Mar. Syst., 143, 62-72, doi:10.1016/j.jmarsys.2014.11.001, 2015.

https://doi.org/10.5194/egusphere-2025-2800
Preprint. Discussion started: 28 August 2025

Pavlov, A.K., Silyakova, A., Granskog, M.A., Bellerby, R.G., Engel, A., Schulz, K.G., and Brussaard, C.P.: Marine CDOM accumulation during a coastal Arctic mesocosm experiment: No response to elevated pCO2 levels, J Geophys Res: Biogeosci. doi:10.1002/2013JG002587, 2014.

Pavlov, A.K., Leu, E., Hanelt, D., Bartsch, I., Karsten, U., Hudson, S.R., Gallet, J.-C., Cottier, F., Cohen, J.H., Berge, J., Johnsen,G., Maturilli, M., Kowalczuk, P., Sagan, S., Meler, J., and Granskog. M.A.: The Underwater Light Climate in Kongsfjorden and Its Ecological Implications. In: Hop, H., Wiencke, C. (eds) The Ecosystem of Kongsfjorden, Svalbard. Advances in Polar Ecology, vol 2. Springer, Cham. https://doi.org/10.1007/978-3-319-46425-1_5, 2019.

Pearlman, S. R., Costa, H. S., Jung, R. A., McKeown, J. J., and Pearson, H. E.: Solids (section 2540), in: Standard Methods for the Examination of Water and Wastewater, edited by: Eaton, A. D., Clesceri, L. S., and Greenberg, A. E., 19th edn., American Public Health Association, Washington, D.C., USA, 2-53–2-64, ISBN 978-0875532292, 1995.

Promińska, A., Cisek, M., and Walczowski, W.: Kongsfjorden and Hornsund hydrography – comparative study based on a multiyear survey in fjords of west Spitsbergen, Oceanologia, 59, 397–412, https://doi.org/10.1016/j.oceano.2017.07.003, 2017.

Promińska, A., Falck, E., and Walczowski, W.: Inter-annual variability in hydrography and water mass distribution in Hornsund, an Arctic fjord in Svalbard. Polar Res. 37, 1495546, 2018.

Rousseaux, C.S., and Gregg, W.W.: Recent decadal trends in global phytoplankton composition. Global Biogeochem Cycles, 29, 1674– 1688. https:// doi.org/10.1002/2015GB005139, 2015.

Sagan, S. and Darecki, M.: Inherent optical properties and particulate matter distribution in summer season in waters of Hornsund and Kongsfjorden, Spitsbergen, Oceanologia, 60, 65–75, https://doi.org/10.1016/j.oceano.2017.07.006, 2018.

Saghravani, S.R., Böttcher, M.E., Hong, W.-L., Kulinski, K., Lepland, A., Sen, A., and Szymczycha, B.: Distributions of in situ parameters, dissolved (in)organic carbon, and nutrients in the water column and pore waters of Arctic fjords (western Spitsbergen) during a melting season, Earth Syst. Sci. Data, 16, 3419–3431, https://doi.org/10.5194/essd-16-3419-2024, 2024.

Saloranta, T.M., and Svendsen, H.: Across the Arctic front west of Spitsbergen: high resolution CTD sections from 1998–2000. Polar Res. 20, 177–184, 2001.

Santos-Garcia, M., Ganeshram, R. S., Tuerena, R. E., Debyser, M. C. F., Husum, K., Assmy, P., and Hop, H.: Nitrate isotope investigations reveal future impacts of climate change on nitrogen inputs and cycling in Arctic fjords: Kongsfjorden and Rijpfjorden (Svalbard), Biogeosciences, 19, 5973–6002, https://doi.org/10.5194/bg-19-5973-2022, 2022.

Sathyendranath, S., Lazzara, L., and Prieur, L.: Variations in the spectral values of specific absorption of phytoplankton, Limnol. Oceanogr., 32, 403–415, https://doi.org/10.4319/lo.1987.32.2.0403, 1987.

Schauer, U., Fahrbach, E., Osterhus, S., and Rohardt, G.: Arctic warming through the Fram Strait: oceanic heat transport from 3 years of measurements. J. Geophys. Res. 109 (C6), C06026, http://dx.doi.org/10.1029/2003JC001823, 2004.

Schellenberger, T., Dunse, T., Kaab, A., Kohler, J., and Reijmer, C.H.: Surface speed and frontal ablation of Kronebreen and Kongsbreen, NW Svalbard, from SAR offset tracking. Cryosphere 9, 2339–2355, 2015.

Sieburth, J. M., Smetacek, V., and Lenz, J.: Pelagic ecosystem structure: heterotrophic compartments of the plankton and their relationship to plankton size fractions, Limnol. Oceanogr., 23, 1256–1263, https://doi.org/10.4319/lo.1978.23.6.1256, 1978.

https://doi.org/10.5194/egusphere-2025-2800
Preprint. Discussion started: 28 August 2025

Skogseth, R., Olivier, L.L.A., Nilsen, F., Falck, E., Fraser, N., Tverberg, V., Ledang, A.B., Vader, A., Jonassen, M.O., Soreide, J., Cottier, F., Berge, J., Ivanov, B.V., and Falk-Petersen, S.: Variability and decadal trends in the Isfjorden (Svalbard) ocean climate and circulation – An indicator for climate change in the European Arctic. Prog. Oceanogr. 187, 102394 https://doi.org/10.1016/j.pocean.2020.102394, 2020.

Smoła, Z.T., Tatarek, A., Wiktor, J.M., Wiktor, J.M.W., Kubiszyn, A., and Węsławski, J.M.: Primary producers and production in Hornsund and Kongsfjorden - comparison of two fjord systems. Polish Polar Res. 38 (3), 351–373. https://doi.org/10.1515/popore-2017-0013, 2017.

Son, Y.-S., and Kim, H.-C.: Empirical ocean color algorithms and bio-optical properties of the western coastal waters of Svalbard, Arctic. ISPRS J. Photogramm. Remote Sens. 139, 272–283. https://doi.org/10.1016/j.isprsjprs.2018.03.024, 2018.

Stoń -Egiert, J., and Kosakowska, A.: RP-HPLC determination of phytoplankton pigments comparison of calibration results for two columns. Mar. Biol. 147, 251–260, https://doi.org/10.1007/s00227-004-1551-z, 2005.

Stramski, D., Babin, M., and Woźniak, S.B.: Variations in the optical properties of terrigenous mineral-rich particulate matter suspended in seawater, Limnol. Oceanogr., 52(6), 2418–2433, https://doi.org/10.4319/lo.2007.52.6.2418, 2007.

Stramski, D., Reynolds, R. I., Kaczmarek, S., Uitz, J., and Zheng, G.: Correction of pathlength amplification in the filter-pad technique for measurements of particulate absorption coefficient in the visible spectral region, Appl. Optics, 54, 6763–6782, https://doi.org/10.1364/AO.54.006763, 2015.

Svendsen, H., Beszczyńska-Møller, A., Hagen, J.O., Lefauconnier, B., Tverberg, V., Gerland, S., Ørbæk, J.B., Bischof, K., Papucci, C., Zajaczkowski, M., Azzolini, R., Bruland, O., Wiencke, C., Winther, J.-G., and Dallmann, W.: The physical environment of Kongsfjorden-Krossfjorden, an Arctic fjord system in Svalbard. Polar Res. 21, 133–166, 2002.

Szeligowska, M., Trudnowska, E., Boehnke, R., and Błachowiak- Samołyk, K.: Dark plumes of glacial meltwater affect vertical distribution of zooplankton in the. Arctic. Sci. Rep. 12, 1—16. https://doi.org/10.1038/s41598-022-22475-8, 2022.

Szeligowska, M., Trudnowska, E., Boehnke, R., Dąbrowska, A. M., Dragańska-Deja, K., Deja, K., Darecki, M., and Błachowiak-Samołyk, K.: The interplay between plankton and particles in the Isfjorden waters influenced by marine- and land-terminating glaciers, Sci. Total Environ., 780, 146491, https://doi.org/10.1016/j.scitotenv.2021.146491, 2021.

Tate, R.D., Benkendorff, K., Ab Lah, R., and Kelaher, B.P.: Ocean acidification and warming impacts the nutritional properties of the predatory whelk, Dicathais orbita, J. Exp. Mar. Biol. Ecol., 493, 7–13. https://doi.org/10.1016/j.jembe.2017.03.006, 2017.

Tripathy, S.C., Varunan, T., Shanmugam, P., Kerkar, A.U., Bhaskar, J.T., Kurian, S., Parli, B.V., and Gauns, M.: Summer variability in bio−optical properties and phytoplankton pigment signatures in two adjacent high Arctic fjords, Svalbard, Int. J. Environ. Sci. Technol., 20, 239–258. doi: 10.1007/s13762-021-03767-4, 2021.

Turner, J. T.: Zooplankton fecal pellets, amrine snow, phytodetritus and the ocean's biological pump, Prog. Oceanogr., 130, 205–248, https://doi.org/10.1016/j.pocean.2014.08.005, 2015.

Uitz, J., Claustre, H., Morel, A., and Hooker, S. B.: Vertical distribution of phytoplankton communities in open ocean: An assessment based on surface chlorophyll, J. Geophys. Res. 111, C08005, https://doi.org/10.1029/2005JC003207, 2006.

https://doi.org/10.5194/egusphere-2025-2800
Preprint. Discussion started: 28 August 2025

Uitz, J., Huot, Y., Bruyant, F., Babin, M., and Claustre, H.: Relating phytoplankton photophysiological properties to community structure on large scales, Limnol. Oceanogr., 53, 614–630, https://doi.org/10.4319/lo.2008.53.2.0614, 2008.

Vidussi, F., Claustre, H., Manca, B.B., Luchetta, A., and Marty, J.C.: Phytoplankton pigment distribution in relations to upper thermocline circulation in the eastern Mediterranean Sea during winter, J. Geophys. Res., 106, 19939–19956, https://doi.org/10.1029/1999JC000308, 2001.

Volkman, J. K. and Tanoue, E.: Chemical and biological studies of particulate organic matter in the ocean, J. Oceanogr., 58, 265–279, https://doi.org/10.1023/A:1015809708632, 2002.

Voss, M., Bange, H. W., Dippner, J. W., Middelburg, J. J., Montoya, J. P., and Ward, B.: The marine nitrogen cycle: Recent discoveries, uncertainties and the potential relevance of climate change. Philos. T. Roy. Soc. B, 368, 20130121, https://doi.org/10.1098/rstb.2013.0121, 2013

Walczowski, W., and Piechura, : Pathways of the Greenland Sea warming, Geophys. Res. Letters, 34(10), L10608, https://doi.org/10.1029/2007GL029974, 2007.

Walczowski, W.: Frontal structures in the West Spitsbergen Current margins. Ocean Sci. 9 (6), 957—975, http://dx.doi.org/10.5194/os-9-957-2013, 2013.

Ward, B.A.; Dutkiewicz, S.; Jahn, O.; Follows, M.J. A Size-Structured Food-Web Model for the Global Ocean. Limnol. Oceanogr. 702, 57, 1877–1891, https://doi.org/10.4319/lo.2012.57.6.1877, 2012.

Włodarska-Kowalczuk, M., Węsławski, J. M., and Kotwicki, L.: Spitsbergen glacial bays macrobenthos – a comparative study, Polar Biol., 20, 66–73, https://doi.org/10.1007/s003000050277, 1998.

Woźniak, B., and Dera, J.: Light Absorption in Sea *Water*. Springer, New York, 2007.

Woźniak, S.B., and Stramski, D.: Modeling the optical properties of mineral particles suspended in seawater and their influence on ocean reflectance and chlorophyll estimation from remote sensing algorithms, Applied Optics, 43(17), 3489-3503, https://doi.org/10.1364/AO.43.003489, 2004.

Woźniak, S.B., Sagan, S., Zabłocka, M., Stoń-Egiert, J., and Borzycka, K.: Light scattering and backscattering by particles suspended in the Baltic Sea in relation to the mass concentration of particles and the proportions of their organic and inorganic fractions, J. Mar. Syst., 182, 79–96, https://doi.org/10.1016/j.jmarsys.2017.12.005, 2018.

Woźniak, S.B., Meler, J., and Stoń-Egiert, J.: Inherent optical properties of suspended particulate matter in the southern Baltic Sea in relation to the concentration, composition and characteristics of the particle size distribution; new forms of multicomponent parameterizations of optical properties, J. Mar. Syst., 229, 10372, https://doi.org/10.1016/j.jmarsys.2022.103720, 2022.

Woźniak, S.B., Litwicka, D., and Stoń-Egiert, J.: Variability and relationships between particle sizes, composition and optical properties of suspended particulate matter in the coastal waters of western Spitsbergen, assessed through measurements of size-fractionated seawater samples. Oceanologia ,66 (4), 66403, https://doi.org/10.5697/EZNP4044, 2024b.

https://doi.org/10.5194/egusphere-2025-2800
Preprint. Discussion started: 28 August 2025

Woźniak, S.B., Litwicka, D., Stoń-Egiert, J., and Stramski, D.: Variability of inherent optical properties of seawater in relation to the concentration and composition of suspended particulate matter in the coastal Arctic waters of western Spitsbergen, J. Mar. Sys., 246, https://doi.org/10.1016/j.jmarsys.2024.104019, 2024a.

Yigiterhan, O., Al-Ansari, E. M., Nelson, A., Abdel-Moati, M. A., Turner, J., Alsaadi, H. A., Paul, B., Al-Maslamani, I. A., Al-Ansi Al-Yafei, M. A., and Murray, J. W.: Trace element composition of size-fractionated suspended particulate matter samples from the Qatari Exclusive Economic Zone of the Arabian Gulf: the role of atmospheric dust, Biogeosciences, 17, 381–404, https://doi.org/10.5194/bg-17-381-2020, 2020.

Zaborska, A., Strzelewicz, A., Rudnicka, P., and Moskalik, M.: Processes driving heavy metal distribution in the seawater of an Arctic fjord (Hornsund, southern Spitsbergen), Mar. Pollut. Bull., 161, 111719, https://doi.org/10.1016/j.marpolbul.2020.111719, 2020.

Zhang, X., Huot, Y., Bricaud, A., and Sosik, H.: Inversion of spectra absorption coefficients to infer phytoplankton size classes, chlorophyll concentration, and detrital matter, Appl. Optics, 54, 5805–5816, https://doi.org/10.1364/AO.54.005805, 2015.